TECHNICAL PROGRESS REPORT

PROJECT TITLE: PROCESSING, MICROSTRUCTURE AND CREEP BEHAVIOR OF Mo-Si-B-BASED INTERMETALLIC ALLOYS FOR VERY HIGH TEMPERATURE STRUCTURAL APPLICATIONS

TYPE OF REPORT: Final

PERIOD OF PERFORMANCE: July 1, 2003 – March 31, 2008

PRINCIPAL: INVESTIGATOR Professor Vijay K. Vasudevan

DATE: October 30, 2008

DoE GRANT NO.: DE-FG26-03NT41793

INSTITUTION: The University of Cincinnati
Department of Chemical and Materials Engineering
501D ERC, Cincinnati, OH 45221-0012

DISCLAIMER

This report was prepared as an account of work sponsored by an agency of the United States Government. Neither the United States Government nor any agency thereof, nor any of their employees, makes any warranty, express of implied, or assumes any legal liability or responsibility for the accuracy, completeness, or usefulness of any information, apparatus, product, or process disclosed, or represents that its use would not infringe privately owned rights. Reference herein to any specific commercial product, process, or service by trade name, trademark, manufacturer, or otherwise does not necessarily constitute or imply its endorsement, recommendation, or favoring by the United States Government or any agency thereof. The views and opinions of authors expressed herein do not necessarily state or reflect those of the United States Government or any agency thereof.

ABSTRACT

This research project is concerned with developing a fundamental understanding of the effects of processing and microstructure on the creep behavior of refractory intermetallic alloys based on the Mo-Si-B system. In the first part of this project, the compression creep behavior of a Mo-8.9Si-7.71B (in at.%) alloy, at 1100 and 1200°C was studied, whereas in the second part of the project, the constant strain rate compression behavior at 1200, 1300 and 1400°C of a nominally Mo-20Si-10B (in at.%) alloy, processed such as to yield five different α-Mo volume fractions ranging from 5 to 46%, was studied. In order to determine the deformation and damage mechanisms and rationalize the creep/high temperature deformation data and parameters, the microstructure of both undeformed and deformed samples was characterized in detail using x-ray diffraction, scanning electron microscopy (SEM) with back scattered electron imaging (BSE) and energy dispersive x-ray spectroscopy (EDS), electron back scattered diffraction (EBSD)/orientation electron microscopy in the SEM and transmission electron microscopy (TEM). The microstructure of both alloys was three-phase, being composed of α-Mo, Mo_3Si and T2-Mo_5SiB_2 phases. The values of stress exponents and activation energies, and their dependence on microstructure were determined. The data suggested the operation of both dislocation as well as diffusional mechanisms, depending on alloy, test temperature, stress level and microstructure. Microstructural observations of post-crept/deformed samples indicated the presence of many voids in the α-Mo grains and few cracks in the intermetallic particles and along their interfaces with the α-Mo matrix. TEM observations revealed the presence of recrystallized α-Mo grains and sub-grain boundaries composed of dislocation arrays within the grains (in Mo-8.9Si-7.71B) or fine sub-grains with a high density of **b** = ½<111> dislocations (in Mo-20Si-10B), which are consistent with the values of the respective stress exponents and activation energies that were obtained and provide confirmatory evidence for the operation of diffusional (former alloy) or dislocation (latter alloy) creep mechanisms. In contrast, the intermetallic phases contained very few dislocations, but many cracks. The relative contributions of the α-Mo and the intermetallic particles to the overall deformation process, including their individual and collective dependence on temperature and strain rate are discussed in light of the present results and those from previous reports.

TABLE OF CONTENTS

Section	Page #
Cover Page	i
Disclaimer	ii
Abstract	ii
List of Tables	iv
List of Figures	iv
1. Introduction	1
2. Executive Summary	2
3. Technical Approach	4
4. Experimental Details	4
5. Results and Discussion	5
5.1 Mo-8.9Si-7.71B (in At.%) Alloy	5
5.1.1 Microstructure of Heat Treated, Undeformed Material	5
5.1.2 Bend Test Results	6
5.1.3 Compression Creep Test Results	7
5.1.4 Microstructure of Crept Samples	11
5.2 Mo-20Si-10B (in At.%) Alloy	14
5.2.1 Microstructure of Undeformed Samples	14
5.2.2 Constant Strain Rate Compression Test Results	17
5.2.3 Microstructure of Deformed Samples	25
5.3 General Discussion	27
6. Conclusions	31
7. References Cited	32
8. List of Publications, Presentations and Students Supported from the Grant	33
8.1 Publications and Presentations	33
8.2 Students Supported Under This Grant	33
9. Acknowledgments	33

LIST OF TABLES

Table 1. Summary of Specimens made from Mo-20Si-10B ingots.

Table 2. Elastic Limit Strength of the Mo-3Si-1B Alloy Obtained by 4-Point Bend Testing

Table 3. Minimum Creep Rate as a Function of Stress at 1200°C for the Mo-3Si-1B Alloys

Table 4. Minimum Creep Rate as a Function of Stress at 1100°C for the Mo-3Si-1B Alloy

Table 5. Data of Strain Rate and Corresponding Plateau Stress at 1200, 1300 and 1400°C for Sample M1 (α-Mo – 5%).

Table 6. Data of Strain Rate and Corresponding Plateau Stress at 1200, 1300 and 1400°C for Sample M2 (α-Mo – 13%).

Table 7. Data of Strain Rate and Corresponding Plateau Stress at 1200, 1300 and 1400°C for Sample C1 (α-Mo – 17%).

Table 8. Data of Strain Rate and Corresponding Plateau Stress at 1200, 1300 and 1400°C for Sample M (α-Mo – 34%).

Table 9. Data of Strain Rate and Corresponding Plateau Stress at 1200, 1300 and 1400°C for Sample C2 (α-Mo – 46%).

Table 10. Values of the Stress Exponent, n, in the Samples at Various Temperatures.

Table 11. Values of the Activation Energy as a Function of Stress in the Samples.

LIST OF FIGURES

Figure 1. (a) Isothermal section at 1600°C of the Mo-rich side of the Mo-Si-B system (from [6]); and (b) microstructure of an extruded and heat-treated (1900°C+ 1400°C) Mo-12Si-12B alloy showing the three phase α-Mo (light) + Mo3Si (dark) + T2 (gray) phases from our previous work.

Figure 2. BSE micrographs showing microstructure of sample MM12-09L cut from a room-temperature-tested bend bar. (a) 500X and (b) 1000X.

Figure 3. BSE micrographs showing microstructure of sample MM12-09L cut from a 1400°C-tested bend bar. (a) 500X and (b) 1000X.

Figure 4. Elastic limit strength as a function of temperature for the Mo-3Si-1B alloy determined using four-point bend testing.

Figure 5. Plots of (a) compressive creep strain versus time and (b) creep rate versus strain at various stress levels for the Mo-3Si-1B alloy tested at 1200°C.

Figure 6. Minimum creep rate versus stress at 1200°C for the Mo-3Si-1B alloy. (a) First minimum and (b) second minimum.

Figure 7. Plot of compressive creep strain versus time at various stress levels for the Mo-3Si-1B alloy tested at 1100°C.

Figure 8. Ln-Ln plot of minimum creep rate versus stress at 1100°C for the Mo-3Si-1B alloy.

Figure 9. Ln(minimum creep rate) versus 10000/T plot for the Mo-3Si-1B alloy tested at 1100 and 1200°C under a stress of 300 MPa.

Figure 10. BSE micrograph showing microstructure of Mo-3Si-1B alloy crept at 1200°C under a stress of 300 MPa.

Figure 11. BF TEM micrographs (a,b) and [011] α-Mo SAD pattern (c) showing the microstructure of the Mo-3Si-1B alloy crept at 1200°C under a stress of 300 MPa.

Figure 12. BF TEM micrographs showing (a) Mo_3Si grain and (b) T2-Mo_5SiB_2 grain (inset [100] T2 SAD pattern) in the Mo-3Si-1B alloy crept at 1200°C under a stress of 300 MPa.

Figure 13. BSE micrographs showing microstructure of sample M1 (a) 500X, (b) 1000X, (c) 2000X and (d) 5000X.

Figure 14. BSE micrographs showing microstructure of sample C1. (a) 200X and (b) 1000X.

Figure 15. BSE micrographs showing microstructure of sample C2. (a) 500X and (b) 1000X.

Figure 16. BSE micrographs showing microstructure of sample M (a) 500X and (b) 1000X.

Figure 17. BSE micrographs showing microstructure of sample M2. (a) 500X and (b) 1000X.

Figure 18. Plots of x-ray intensity versus 2θ recorded from various samples. (a) C1 and (b) C2.

Figure 19. (a) Orientation map and (b) corresponding inverse pole figure recorded from an α-Mo region in sample C2.

Figure 20. Plot of stress versus strain during the jump test at 1200°C for sample C1.

Figure 21 Plots showing the variation in the plateau stress with % α-Mo at strain rates of (a) 10^{-6} s^{-1}, (b) 10^{-5} s^{-1} and (c) 10^{-4} s^{-1}.

Figure 22. Plot of ln(strain rate) versus ln(stress at 1200, 1300 and 1400°C. (a) sample M2 and (b) Sample C1.

Figure 23. Plot of ln(strain rate) versus ln(stress at 1200, 1300 and 1400°C. (a) sample M and (b) Sample C2.

Figure 24. Plot of stress exponent values versus α-Mo volume fraction for the samples tested at 1200, 1300 and 1400°C.

Figure 25. Plot of ln(strain rate) versus $10^4/T$ at stresses of 400, 500 and 600 MPa for sample C2, allowing determination of the activation energy, Q.

Figure 26. Plot of activation energy, Q, versus α-Mo volume fraction at different stress levels for samples tested at 1200, 1300 and 1400°C.

Figure 27. BSE micrographs showing overall microstructure of a C2 sample deformed at a single strain rate of 10^{-5} s^{-1} at 1200°C.

Figure 28. (a) Orientation map, (b) corresponding inverse pole figure and (c) distribution of grain/sub-grain sizes recorded from an α-Mo region in sample C2 that had been subjected to the jump test at 1400°C.

Figure 29 (a) [110] and (b) [111] SAD patterns recorded from the α-Mo region in sample C2 that had been subjected to the jump test at 1400°C.

Figure 30. TEM micrographs recorded from sample C2 that had been subjected to the jump test at 1400°C. (a) through (e) were recorded from the α–Mo region showing dislocations and sub-grain boundaries: (a) BF, **g**=0-11, (b) WBDF, **g**=0-11, (c) BF, **g**=101, (d) BF, **g**=-101and (e) BF, **g** 110; (f) BF micrograph of a Mo_3Si particle showing practically no dislocations.

Figure 31. BF TEM micrographs recorded from sample C2 that had been subjected to the jump test at 1300°C. (a) through (e) were recorded from the α–Mo region showing dislocations and sub-grain boundaries: (a) low magnification, (b) **g**=0-11, (c) **g**=101, (d) **g**=-101and (e) **g** 110; (f) micrograph of a Mo_3Si particle showing practical very few dislocations.

1. INTRODUCTION

There is a constantly increasing demand for improved high-temperature engineering materials for applications in advanced energy, power and transportation systems. The new generation of energy/power systems demand very high thrust-to-weight ratios, which necessitates use of components with high strength, creep, fatigue and oxidation resistance at temperatures in the range of 1000 to 1600°C. These temperature requirements are clearly beyond the capabilities of many metallic materials currently available, including superalloys and aluminides based on nickel and titanium. Consequently, development of new high temperature materials capable of use over this temperature range is one of the critical pacing technologies. In addition to the temperature requirements, other critical materials properties cannot be compromised, including environmental resistance (oxidation and hot corrosion), adequate low temperature fracture toughness or ductility, elevated temperature strength (tensile and creep), and thermal-mechanical fatigue resistance.

In recent years, considerable attention has been focused on alloys based on the Mo-Si-B system [1-23] for these very high temperature (>1200°C) structural applications because of their possibility of offering a multiphase design concept involving hard, intermetallic second phases with a ductile matrix for balanced high temperature strength and toughness, coupled with excellent oxidation resistance, high melting points, moderate densities and high elastic moduli [1-23]. Indeed, studies of phase relations and microstructure have shown that the alloy compositions having the best potential for balanced properties through microstructure manipulation lie in the three-phase region (Figure 1) composed of the intermetallic phases T2-Mo_5SiB_2 and Mo_3Si in an α-Mo solid solution matrix [6-8]. The oxidation resistance of candidate alloys is excellent at temperatures above 1000°C, which is achieved through the formation of an adherent and protective SiO_2 scale [2-4,9,10].

The mechanical properties of this class of alloys have also been studied [11-23]. The Mo_3Si and T2 intermetallic phases retain high strengths up to 1400°C [13-16], but are extremely brittle, with room temperature fracture toughness values on the order of 3 MPa-√m [13]. Substantial improvements in the room temperature fracture toughness are obtained, to values as high as 10 MPa, in three phase α-Mo+Mo_3Si+T2 compositions, wherein the α-Mo provides ductile phase toughening by plastic stretching and crack trapping [18,19]. Further increases (to ~15 MPa √m) have also been made possible using novel vacuum annealing and powder metallurgical processing to produce microstructures with continuous α-Mo layers surrounding the intermetallic phases [21]. Fracture toughness values of ~20 MPa√m are obtained at elevated temperatures [18].

There have been a few studies of the high temperature strength of the three-phase alloys. The high temperature strength of a near 50:50 α-Mo: T2 volume fraction alloy was found [13] to be comparable to that of ultrahigh temperature W-Re-ThO_2 alloys. An alloy with 38 vol.% Mo, 32 vol.% Mo_3Si and 30 vol. % T2 had strength levels of 400-500 MPa at 1200°C [18]. Studies of the creep properties are very limited. Recently, Schneibel [22], using constant strain rate (10^{-5} s^{-1}) compression tests, estimated the high temperature creep strength of three-phase α-Mo+Mo_3Si+T2 materials that had been processed by different routes and with and without alloying additions of Nb and W. Although not strictly a creep test, the results were useful for obtaining both semi-quantitative estimates of the creep strength (defined as the stress corresponding to 2% plastic strain) and a qualitative understanding of the effects of microstructure and alloying. The alloy composition, topology and scale of microstructure were found to have a profound influence on the creep strength, with coarser microstructures containing isolated α-Mo particles exhibiting higher creep strengths than those with a continuous α-Mo matrix. More recently, Alur *et al.* [23] that the high temperature compression strength of two/three-phase Mo-Si-B alloys r the 1000-1400°C range was superior to TZM and that the deformation in the temperature-strain rate space evaluated was largely controlled by the α-Mo matrix. Despite these studies, the mechanisms governing the high temperature creep behavior and the influences of variations in the microstructure in these alloys are still not fully understood.

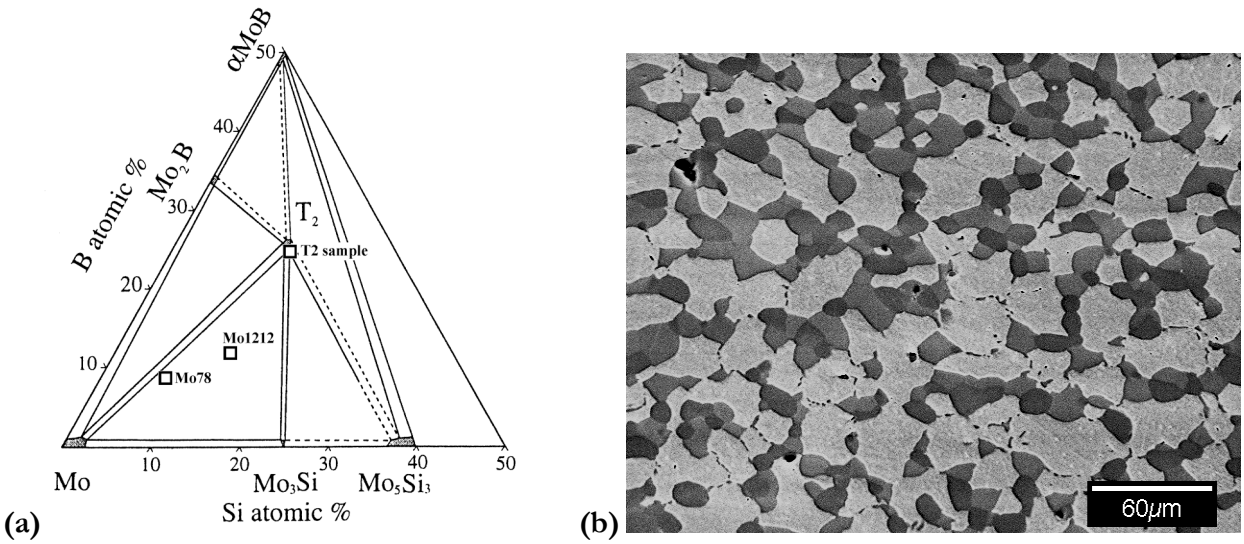

Figure 1—(a) Isothermal section at 1600°C of the Mo-rich side of the Mo-Si-B system (from [6]); and (b) microstructure of an extruded and heat-treated (1900°C+ 1400°C) Mo-12Si-12B alloy showing the three phase α-Mo (light) + Mo3Si (dark) + T2 (gray) phases from our previous work.

This research project combines a novel processing, experimental and modeling approach, with quantitative analysis of the influences of microstructure, in the study of the creep behavior of representative Mo-Si-B alloys. The aim is to gain insight into the high-temperature creep behavior of these materials, including the effects of microstructure and the associated deformation, damage and failure features. This project, which is closely coupled with ongoing activities at the Air Force Research Laboratory (AFRL) and Oak Ridge National Laboratory (ORNL) on these materials, focuses on three key areas to address issues related to the creep behavior: 1) basic materials processing and microstructural studies of selected alloys (Mo-3Si-1B and Mo-20Si-10B); 2) evaluation of the creep phenomenology and establishment of the constitutive behavior of the three-phase alloys, including the effects of microstructural variations; and 3) modeling of the creep behavior based on analysis of associated creep/compression data, deformation mechanisms, damage processes and microstructural parameters. An important component of this research is to perform a detailed analysis of microstructures utilizing modern electron optical techniques, to provide quantitative information on aspects such as volume fraction, length scales, morphology and distribution of the second-phase intermetallics, the nature of their interfaces with the matrix, and the deformation, damage and failure processes during creep. This information, together with those of the creep properties and phenomenology are utilized to rationalize and model the observed creep behavior.

2. EXECUTIVE SUMMARY

This research project is concerned with developing a fundamental understanding of the effects of processing and microstructure on the creep behavior of refractory intermetallic alloys based on the Mo-Si-B system. These materials are being considered for very high temperature structural applications. In the first part of this project, the microstructure and creep properties of a three-phase Mo-3 wt.% Si-1 wt.% B (Mo-8.9Si-7.71B in at.%) alloy that was produced using a powder metallurgy and supplied by UES/AFRL was studied. Microstructural observations using back-scattered electron imaging in a scanning electron microscope revealed that this alloy was three-phase, consisting of α-Mo, Mo_3Si and T2-Mo_5SiB_2 phases, with the combined volume fraction of the latter two being ~30%. Samples for mechanical testing were prepared by electro discharge machining. Bend tests revealed that the elastic limit strength of the alloy remained quite high until 1200°C with a value of 800MPa, but dropped rapidly thereafter to a value of 220 MPa at 1400°C. Compression creep tests were conducted under inert atmosphere at 1200°C and 1100°C at stress levels

ranging from 100 to 500 MPa in an Applied Test Systems creep frame equipped with computerized data acquisition. The results showed that the creep rates at 1200°C were quite high and the data of creep strain rate versus time or strain displayed two minima, one at small strains and the second at much larger strains. The former minima varied linearly from a value of 4.23 x 10^{-5} min^{-1} at 250 MPa to 7.95 x 10^{-4} min^{-1} at 500 MPa, whereas the latter were 3.58 x 10^{-5} min^{-1} and 8.04 x 10^{-5} min^{-1} at the same stress levels, respectively. The stress exponent from the data corresponding to the first minima was determined to be ~4.26, which suggests that dislocation climb-glide creep dominates the creep process in the early stages. This value of the stress exponent is in the range of 2-7 reported for similar alloys by other investigators. The stress exponent determined from the second minimum creep rate data was ~1.18, which is near the value of 1 expected for diffusional creep and recrystallization mechanisms. At 1100°C, the minimum creep rates varied linearly with stress from 1.66x10^{-7} min^{-1} at 100 MPa to 2.13x10^{-6} min^{-1} at 300 MPa; the corresponding stress exponent was determined to be ~2.26, which suggests that both diffusional and dislocation mechanisms contribute to the overall creep process. The activation energy, Q, for creep was determined to be ~525 kJ/mole, which is somewhat higher than the value of 400 kJ/mole reported for self diffusion in α-Mo. Microstructural observations of post-crept samples indicated shape change and deformation of the α-Mo grains, together with the presence of many voids in these grains. A few cracks in the intermetallic particles and along their interfaces with the α-Mo matrix were also observed. TEM observations of the crept samples revealed the presence of recrystallized α-Mo grains containing small-angle sub-grain boundaries made up of dislocation arrays. A few dislocations and sub-grains were also noted within the Mo_3Si and T2 grains. These observations suggest that the bulk of the deformation and strain during creep is carried by the α-Mo.

In the second part of this project, the microstructure and high temperature compression behaviorof samples of a nominally Mo-20Si-10B (in at.%) alloy that had been processed to produce microstructures with five different volume fractions of the α-Mo phase and received from ORNL were studied. X-ray diffraction and microstructural observations revealed that the samples were three-phase, consisting of α-Mo, Mo_3Si and T2-Mo_5SiB_2 phases, with the volume fraction of the α-Mo phase varying from 5 to ~46%. Constant strain rate (10^{-6} to 10^{-4} s^{-1}) compression tests were conducted at 1200, 1300 and 1400°C and the plateau stresses corresponding to these strain rates were measured from the stress-strain curves. The results showed that the stresses required to maintain a given strain rate increased with a decrease in temperature and generally decreased with an increase in the α-Mo volume fraction, particularly at the lower temperatures; this stress did not vary much with % α-Mo at 1400°C and the two higher strain rates (10^{-5} and 10^{-4} s^{-1}). The values of the stress exponents determined from the data ranged from ~3-9, depending on temperature and α-Mo volume fraction, with those at 1200°C lying between 7-9 regardless of the α-Mo volume fraction, whereas those at 1400°C changing from 3 to ~6 with an increase in α-Mo volume fraction. The n values at 1300°C ranged from 5-7, i.e. were between those at 1200 and 1400°C and showed a similar trend with α-Mo volume fraction as in the 1200°C data. These stress exponent values suggest that dislocation climb-glide mechanisms dominate the creep deformation process. The activation energy, Q, for creep was determined to range from ~200-600 kJ/mole, depending on the stress level and volume fraction of α-Mo. The values in the higher α-Mo volume fraction samples at lower stresses are ~400 kJ/mole, near that for self-diffusion in α-Mo, but drop to ~200-300 kJ/mole at higher stresses. In contrast, in the lower α-Mo volume fraction samples, the Q values at lower stresses are ~600kJ/mole, but drop to ~400 kJ/mole at higher stresses. EBSD/orientation imaging microscopy of the deformed samples in the SEM revealed that the α-Mo regions were subdivided into fine 1 μm size grains/sub-grains. TEM observations provided confirmation for fine sub-grains, whose boundaries were composed of arrays of dislocations, and the presence of a high density of ½<111> dislocations within the sub-grains of the α-Mo. In contrast, the intermetallic phases contained very few dislocations. These observations suggest that the bulk of the deformation and strain during high temperature compression is carried by the α-Mo, with dislocation creep/climb-glide mechanisms being operative, with the intermetallic particles providing a varying level of constraint to the deformation and strain localization depending on temperature and strain rate, which is reflected in the flow/plateau stresses and stress exponents.

3. TECHNICAL APPROACH

The basic strategy utilized in this project is to 1) study the microstructure and creep behavior of a representative three-phase α-Mo+T2-Mo_5SiB_2+Mo_3Si alloy, namely Mo-8.9 at.% Si-7.71 at.% B (Mo-3Si-1B in wt.%) and 2) determine the effects of volume fraction of the constituent phases (α-Mo + intermetallics) and hence microstructure on the high temperature compression behavior of a Mo-20 at.% Si-10 at.% B (Mo-7.61-1.46B in wt.%) alloy. In the first part, the bend strength of the alloy as a function of temperature to 1400°C was determined, followed by the study of the compression creep behavior at 1100 and 1200°C over a range of stresses and the accompanying microstructural changes. In the second part, rather than determining the creep rates under constant load as in a conventional creep test, the approach utilized was to conduct constant strain rate compression tests at temperatures from 1200 to 1400°C and then determine the corresponding stresses required to maintain these strain rates. In this way, data of the stress, temperature and microstructure dependence of creep rates could be obtained rapidly. The microstuructures before and after high temperature compression were studied to ascertain possible creep and damage mechanisms. Lastly, the results of this project are compared with those of previous reports and discussed in detail.

4. EXPERIMENTAL DETAILS

For the first part of this project, a three-phase α-Mo + T2 +Mo_3Si Mo-8.9Si-7.71B (in at.%) alloy was received from UES/AFRL (Dayton, OH). A powder metallurgy route was used by Plansee (Austria) to process this material into bulk form. Thermal influences on microstructure evolution were studied and conditions were established to obtain a well-defined three-phase microstructure. A set of four-point bend test samples were prepared by EDM and the bend strengths determined at 1000°C, 1200°C and 1400°C. Samples measuring 5x5x10 mm were sectioned using electro discharge machining (EDM) for the creep tests. Considerable effort was directed toward getting the creep testing equipment and associated hardware/software at AFRL operational. The creep tests were conducted on a creep frame constructed by Applied Testing Systems. The creep frame consists of lever arm system for loading with an automated ram system that allows for maintaining constant stress or strain rate, a furnace for elevated temperature testing, and an environmental chamber for testing in controlled atmospheres. During experiments, time, displacement, temperature, and applied load measurements are performed by a data acquisition system and collected by a PC. Compression creep tests were conducted on the Mo-3Si-1B alloy samples at 1100 and 1200°C and stress levels ranging from 100 to 500 MPa. Data on creep strain and creep rate with time under these conditions has been obtained.

For the second part of this project, samples of a nominally Mo-20Si-10B (in at.%) alloy that had been processed to produce microstructures with five different volume fractions of the α-Mo phase and received from Dr. Joaquim Schneibel from ORNL were studied. The processing steps included first crushing of the alloy ingot to powder, followed by heat treatment in vacuum at 1600°C for various times for Si removal and then hot isostatic pressing (HIP) of the powders to full consolidation at 1600°C and 210 MPa for 2h [21]. Details of the sample ID, powder size, time at 1600°C in vacuum and the α-Mo volume fraction (determined by quantitative metallography) are provided in Table 1. The samples received were rectangular with dimensions of 4.4 x 4.4 x 6.9 mm.

Table 1. Summary of Specimens made from Mo-20Si-10B ingots.

Specimen ID	Powder size (μm) prior to Si removal	Time at 1600°C in vacuum	Alpha-Mo Volume Fraction, %, metallographic
M1	45 - 90	4h	5
M	45 - 90	20h	34

C1	90-180	120h	17.0
M2	45 - 90	40h	13.1
C2	75 - 180	168h	45.8

Creep rate controlled compressive tests on the samples of the Mo-20Si-10B master alloy were conducted at Brown University on a servo-hydraulic testing machine with the strain rate 10^{-6}, 10^{-5}, and 10^{-4} s^{-1} at 1200, 1300, and 1400°C. Prior to testing the ends of the samples were polished so as to be flat and parallel to each other, and then placed vertically between silicon carbide platens in a furnace with a vacuum better than 10^{-6}Pa. Two kinds of tests were conducted: 1) jump test, in which strain rate was changed from 10^{-6} to 10^{-5} s^{-1} and then to 10^{-4} s- after each steady load state was reached over a strain/deformation of ~4-6%, at each strain rate and the whole test was performed continuously at the same temperature; and 2) single test, in which a constant strain rate of 10^{-5} s- was maintained at each temperature. Load-displacement data were monitored and tests were performed till a steady-state load with increasing displacement was attained. From the data, the plateau stress, corrected for change in sample dimensions, at each strain rate and at a given temperature was determined and the data plotted.

The microstructures of the samples of the Mo- and Mo-20Si-10B in various conditions were characterized by scanning (SEM) and transmission electron microscopy (TEM). The microstructures were observed in a FEI XL30 FEG-ESEM using back-scattered electron (BSE) imaging. The chemical compositions of phases present were analyzed by energy dispersive x-ray spectroscopy (EDS) using an EDAX Genesis 4000 EDS system attached to the SEM. In addition, electron back scattered diffraction (EBSD)/ orienation imaging microscopy (OIM) observations of the samples was conducted in the same SEM to obtain information on grain size, texture and distribution of phases. Thin foils for TEM were prepared by electrical discharge machining (EDM) thin strips from the tested samples, then punching 3-mm diameter disks, followed by dimpling using a Fischione Model 150 dimple grinder and then ion-milling to perforation using a Fischione Model 1010 low-angle ion milling system. The foils were observed in a Philips CM20 TEM operated at 200 kV and photographs under bright field (BF), dark field (DF), weak-beam dark field (WBDF) and selected area diffraction (SAD) modes were recorded. The chemical composition of phases present was also analyzed using an EDAX Genesis 2000 energy dispersive x-ray spectroscopy (EDS) system attached to the same TEM.

5. RESULTS AND DISCUSSION

5.1 Mo-8.9Si-7.71B (in At.%) Alloy

5.1.1 Microstructure of Heat Treated, Undeformed Material

The thermo mechanically processed materials of the Mo-3Si-1B alloy received from Plansee were heat treated at 1700°C, 24h prior to bend testing. The microstructures of samples cut from the ends of the bend test bars were observed. The images of the microstructure were obtained for two un-crept samples along with EDS measurements for identification of the three constitutive phases expected to be present. The microstructure of two samples, namely MM12-09L and MM12-14L, was investigated to ensure that the microstructure was unaffected by the temperature exposures during the bend tests. The former sample was cut from the end of a bend test specimen tested at room temperature, whereas the latter was cut from the end of a bend test specimen tested at 1400°C. The microstructures of these samples are shown in Figures 2 and 3, respectively.

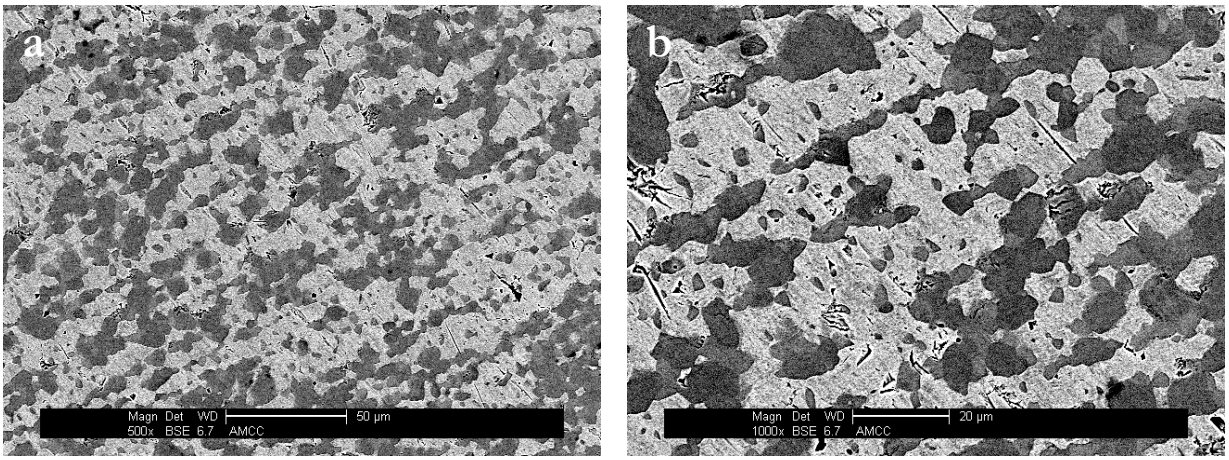

Figure 2—BSE micrographs showing microstructure of sample MM12-09L cut from a room-temperature-tested bend bar. (a) 500X and (b) 1000X.

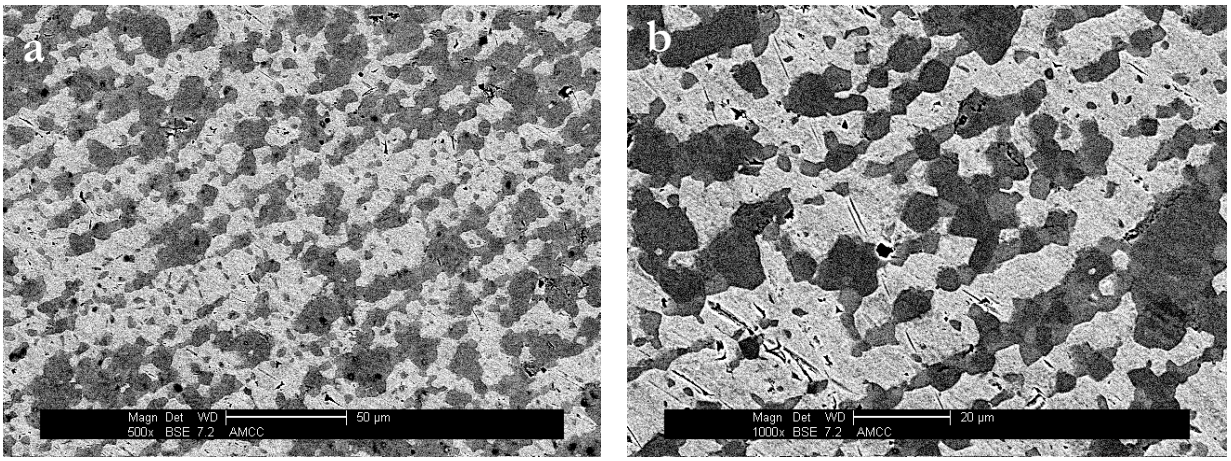

Figure 3—BSE micrographs showing microstructure of sample MM12-09L cut from a 1400°C-tested bend bar. (a) 500X and (b) 1000X.

In both sets of samples, the microstructures were essentially the same and were composed of three phases appearing in bright, gray and dark contrast, which were confirmed by EDS analysis as being the α-Mo, Mo_3Si and T2-Mo_5SiB_2 phases, respectively. Some grain alignment of the α-Mo and intermetallic particles is evident as a result of extrusion. The intermetallic particles showed a tendency for clustering together and bands of these were separated by the α-Mo regions. The average size of Mo_3SI and T2 particles was ~10 µm and their total volume fraction was estimated to be ~30%.

5.1.2 Bend Test Results

Four-point bending tests were conducted on this material using facilities at the AFRL and the results of the elastic limit strength shown in the Table 1 and plotted in Figure 3. The room temperature strength could not be ascertained, because of premature brittle failure of the sample. The results obtained at the other temperatures (Table 2 and Figure 4) show that the strength of the alloy remains high up to 1200°C, with a value of 800 MPa, and then rapidly drops at higher temperatures to a much lower value of 220 MPa at 1200°C. This drop in strength was also accompanied by significant plasticity, which was not seen at the lower temperatures.

Table 2. Elastic Limit Strength of the Mo-3Si-1B Alloy Obtained by 4-Point Bend Testing

Temperature (°C)	Elastic Limit Strength (MPa)
1000	1000
1200	800
1400	220

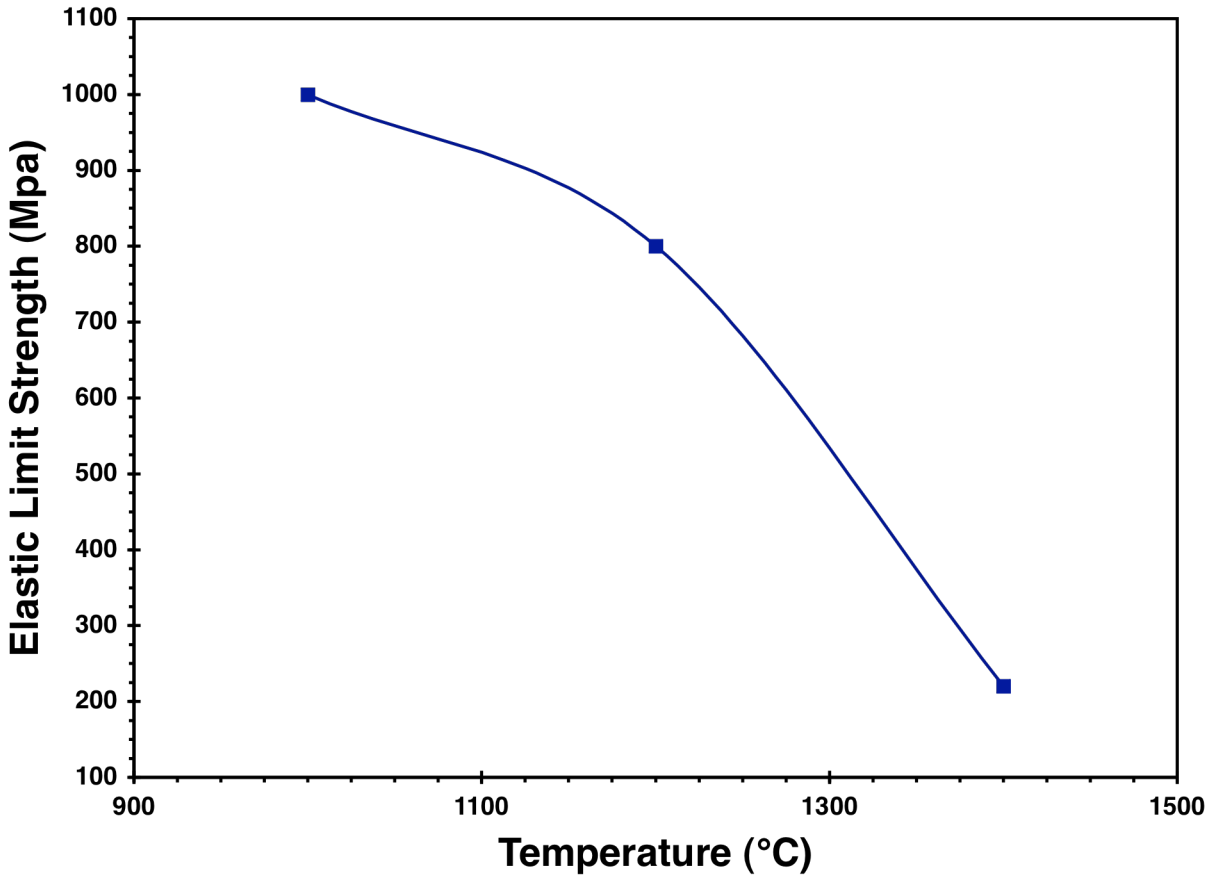

Figure 4—Elastic limit strength vs temperature for the Mo-8.9Si-7.71B alloy determined using four-point bend testing.

5.1.3 Compression Creep Test Results

The results of compression creep tests on the Mo-3Si-1B alloy at 1200°C at stress levels varying from 250 to 500 MPa are shown in Figure 5 in the form of creep strain versus time (Figure 5(a)) and creep strain rate versus strain (Figure 5(b)) plots. As can be seen in Figure 5, the creep curves show three distinct stages, an initially non-linear part with a greater slope/rate followed by a minimum at small strains, then an increase, followed by a second minimum at much larger strains. These features are particularly evident at the higher stress levels. Furthermore, with an increase in the applied stress both the rate of strain and magnitude of strain increases appreciably, with values of the latter of ~50% at 500 MPa at the end of the test. The minimum creep rate corresponding to the first and second minima determined from these data are shown as a function of stress in Table 3 and plotted in Figure 6.

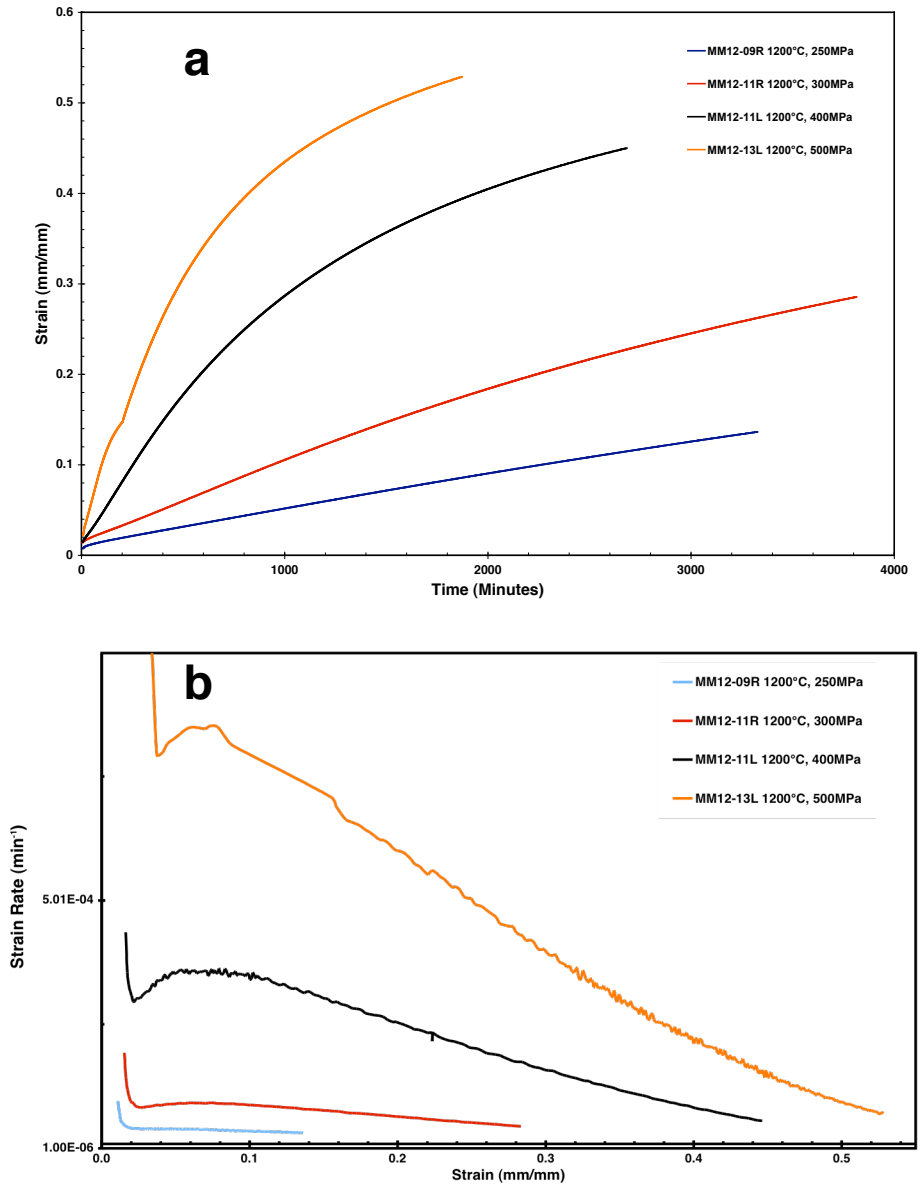

Figure 5—Plots of (a) compressive creep strain versus time and (b) creep rate versus strain at various stress levels for the Mo-8.9Si-7.71B alloy tested at 1200°C.

Table 3. Minimum Creep Rate as a Function of Stress at 1200°C for the Mo-8.9Si-7.71B Alloy.

Stress (MPa)	Minimum Creep Rate (min^{-1})	
	First Minimum	Second Minimum
250	4.23×10^{-5}	3.38×10^{-5}
300	8.39×10^{-5}	4.86×10^{-5}
400	2.97×10^{-4}	6.07×10^{-5}
500	7.95×10^{-4}	8.04×10^{-5}

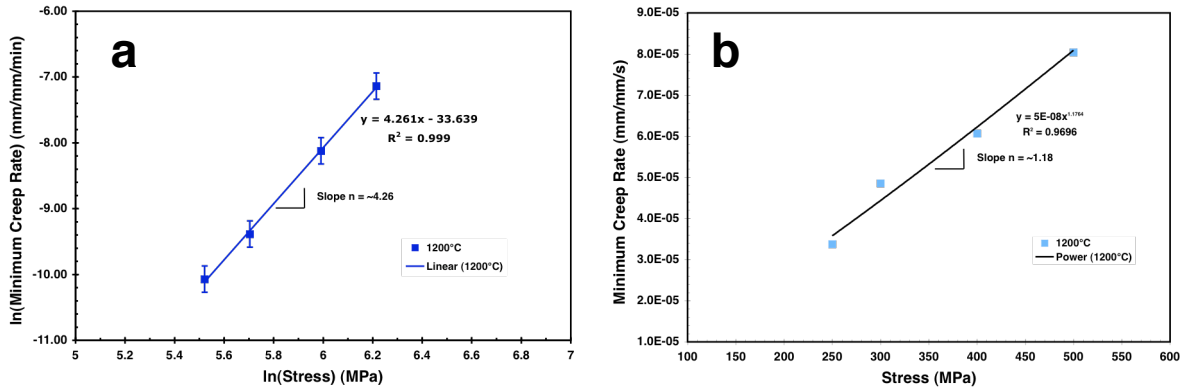

Figure 6—Minimum creep rate versus stress at 1200°C for the Mo-8.9Si-7.71B alloy. (a) First minimum and (b) second minimum.

The data in Table 3 and Figure 6 show that the minimum creep rate corresponding to both mimina increases with stress and that the creep behavior obeys the Mukherjee-Sherby-Dorn creep law of the type:

$$\dot{\varepsilon}_{\min} = A\sigma^{n} \exp\left(-\frac{Q}{RT}\right) \qquad (1)$$

Furthermore, a natural log-log plot of the minimum creep rate versus stress data corresponding to the first minimum, Figure 6(a), gives an excellent straight line fit, yielding a stress exponent of ~4.26. This value is in the range of 3-5 expected for power law/dislocation creep, suggesting that this (i.e., dislocation climb-glide) is the dominant creep mechanism in the initial stages of creep in this alloy. This is in agreement with previous studies on compressive deformation/creep of three-phase α-Mo + Mo_3Si + T2 alloys, where stress exponents ranging from 2.1-3.9 [22] and from 2.5-7.1 [23] have been reported, though the compositions and hence volume fraction of the intermetallic phases of the alloys studied differ from that of the present work. On the other hand, plotting the minimum creep rate corresponding to the second minimum versus stress, Figure 6(b) and an excellent power law fit to this data yields a stress exponent of 1.18, which is close to the value of 1 expected for diffusional (Nabarro-Herring or Coble) creep and/or recrystallization. These results suggest that diffusional and recrystallization processes dominate creep at the later stages.

The compression creep curves of the samples tested at 1100°C at 100, 150 and 300 MPa are shown in Figure 7. Only a single minimum in the creep rate versus strain plot was detected, with the corresponding values shown in Table 4. A natural log-log plot of minimum creep rate versus stress is shown in Figure 8 and a straight line fit to this data yields a stress exponent of 2.26. This value is in the range reported for other Mo-Si-B alloys by previous investigators [22,23] and suggests that both diffusional and dislocation creep processes contribute to the overall creep rate at this temperature over the stress range studied. Furthermore, from a plot of the ln(minimum creep rate) at 1100 and 1200°C vs 10000/T, Figure 9, the activation energy for creep is obtained as 525 kJ/mole. This value is somewhat higher than that reported for other Mo-Si-B alloys by previous investigators [1,2] and for self-diffusion in α-Mo (400 kJ/mole).

Table 4. Minimum Creep Rate as a Function of Stress at 1100°C for the Mo-3Si-1B Alloy

Stress (MPa)	Minimum Creep Rate (min^{-1})
100	1.66×10^{-7}
150	6.36×10^{-7}
300	2.13×10^{-6}

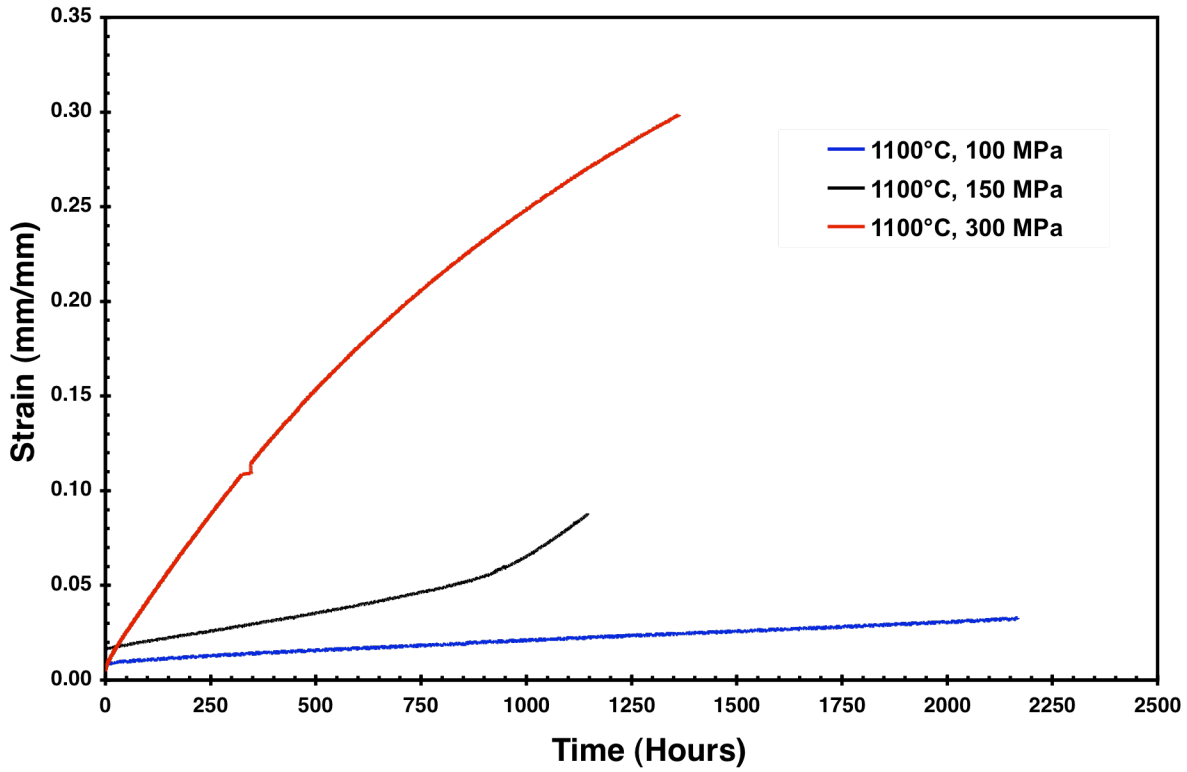

Figure 7—Plot of compressive creep strain versus time at various stress levels for the Mo-3Si-1B alloy tested at 1100°C.

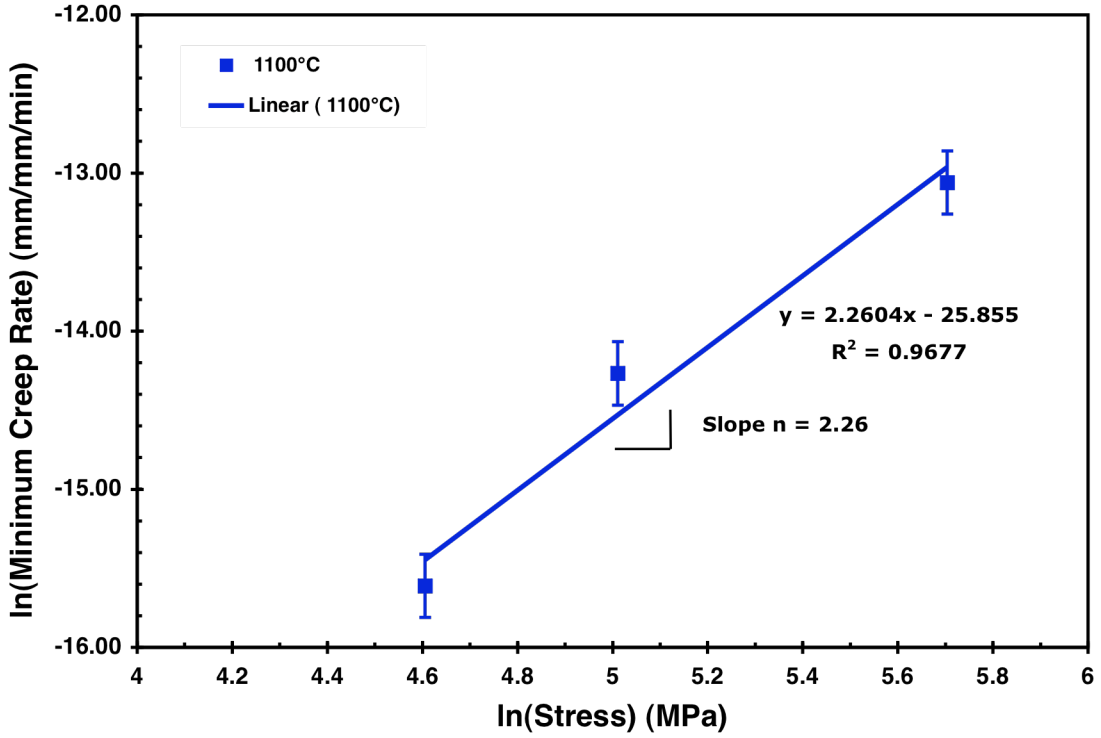

Figure 8—Ln-Ln plot of Minimum creep rate versus stress for the Mo-3Si-1B alloy tested at 1100°C.

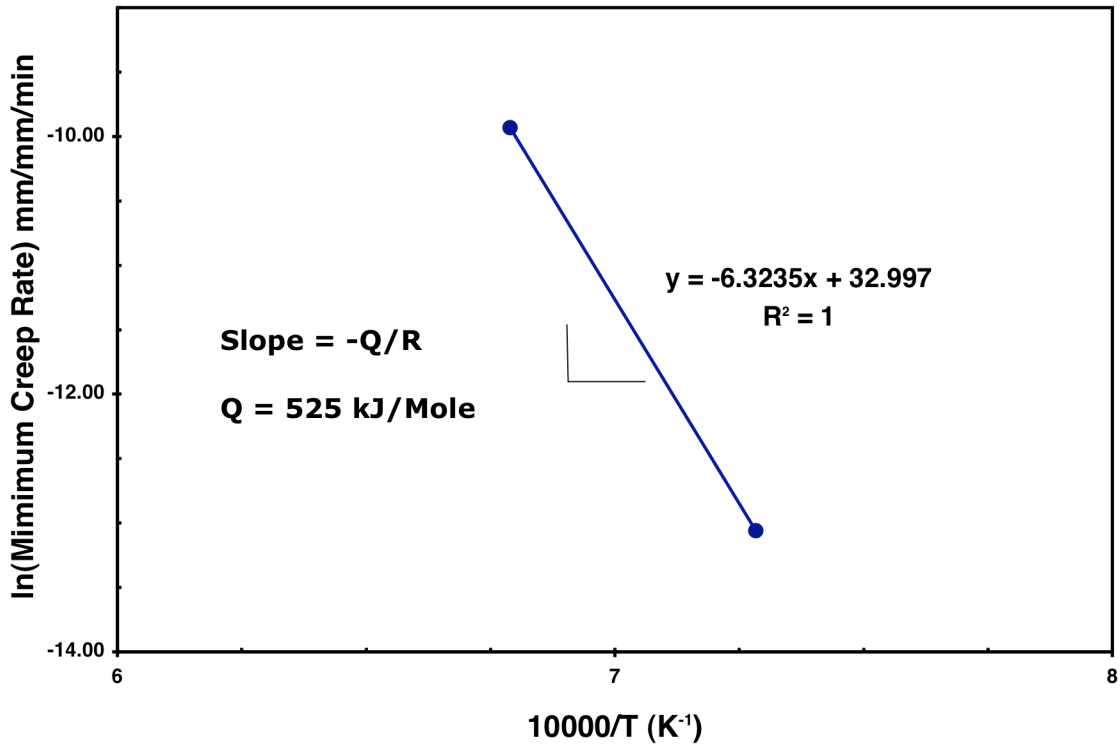

Figure 9—Ln(Minimum Creep Rate) versus 10000/T plot for the Mo-3Si-1B alloy tested at 1100 and 1200°C under a stress of 300 MPa.

5.1.4 Microstructure of Crept Samples

Visual examination of the crept samples showed evidence for barreling, but no macro cracks or other defects were visible. Specimens were sectioned from the crept samples in a direction normal to the compression axis, metallographically prepared and their microstructures observed using BSE imaging in the SEM. Representative BSE micrographs of samples crept at 1200°C at stresses of 250 MPa and 300 MPa are shown in Figures 10(a) and 10(b), respectively.

A change in shape of the α-Mo grains can be clearly seen, whereas the Mo_3Si and T2 particles appear relatively unchanged compared with the uncrept material. Furthermore, many voids and cracks can be seen within the α-Mo grains and a few are present within the intermetallic particles and along their interfaces with the α-Mo grains. These observations suggest that the bulk of the deformation and strain is carried by the α-Mo.

TEM micrographs of the sample creep-tested at 1200°C under a stress of 300 MPa are shown in Figures 11 and 12. These micrographs indicate that the bright α-Mo regions seen in the BSE micrograph in Figure 10 are actually composed of recrystallized grains of α-Mo, ~1.5 μm in size. These grains also contain a relatively low dislocation density, as well as low-angle sub-grain boundaries made up of dislocation arrays (Figure 11) The Mo_3Si and T2 grains contain a few dislocations, Figure 12. In addition, the latter grains are composed of many subgrains. These various observations indicate that the majority of the strain during creep is carried by the α-Mo grains and that at large strains recrystallization of the latter is the predominant creep mechanism, consistent with the observed stress exponent near 1.

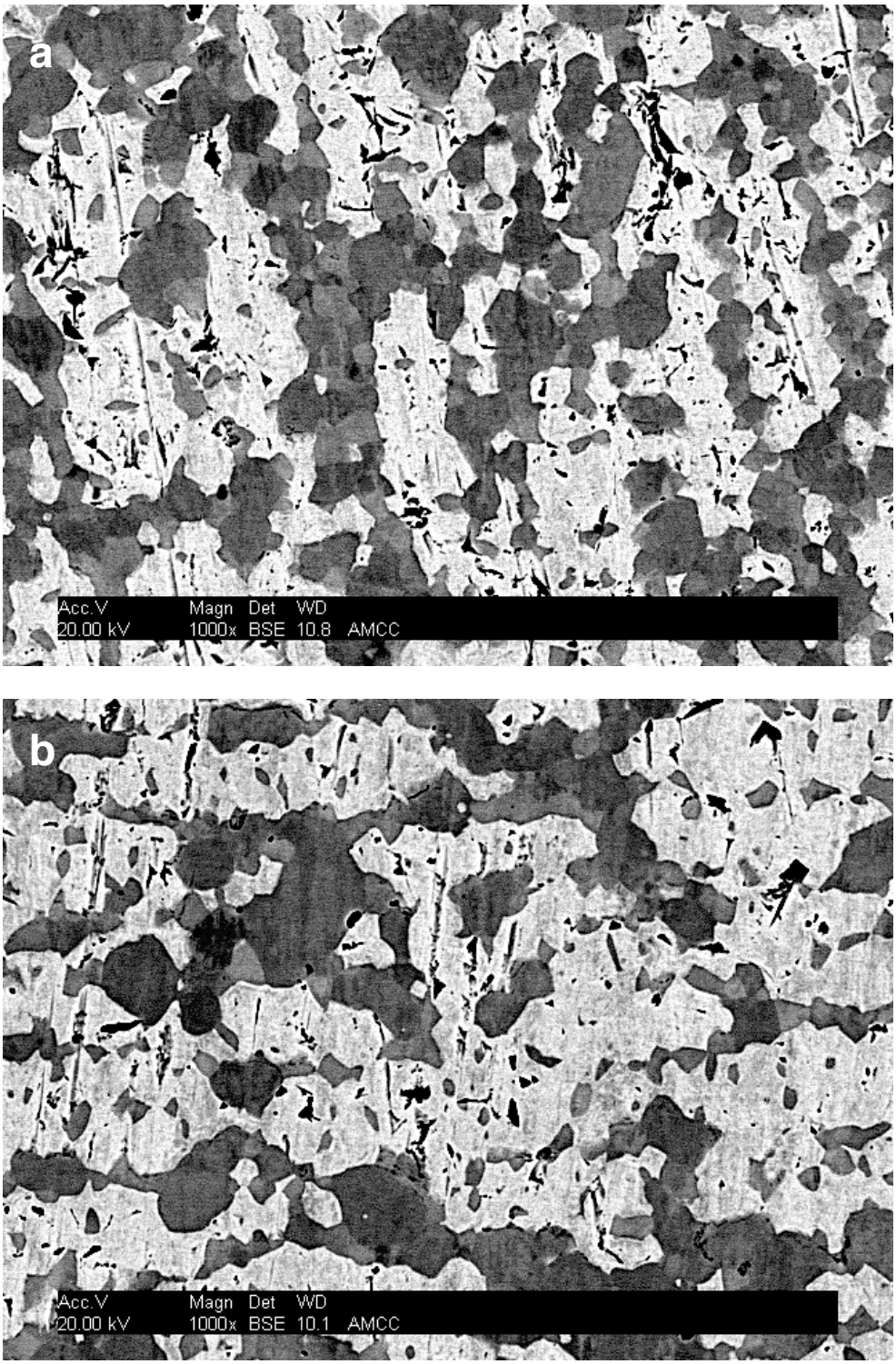

Figure 10—BSE micrographs showing microstructure of Mo-3Si-1B alloy crept at 1200°C under a stress of (a) 250 MPa and (b) 300 MPa.

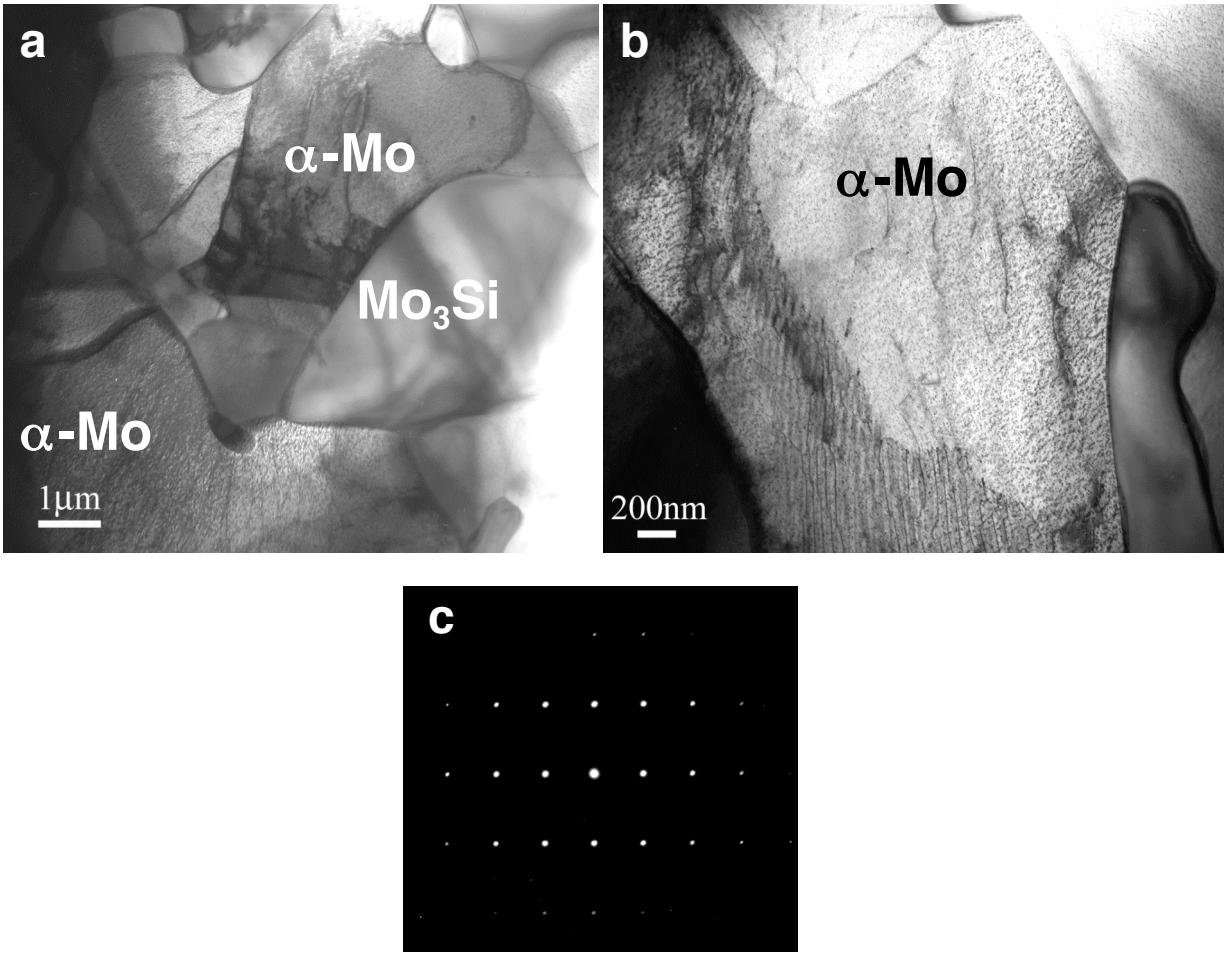

Figure 11—BF TEM micrographs (a,b) and [011] α-Mo SAD pattern (c) showing the microstructure of the Mo-3Si-1B alloy crept at 1200°C under a stress of 300 MPa.

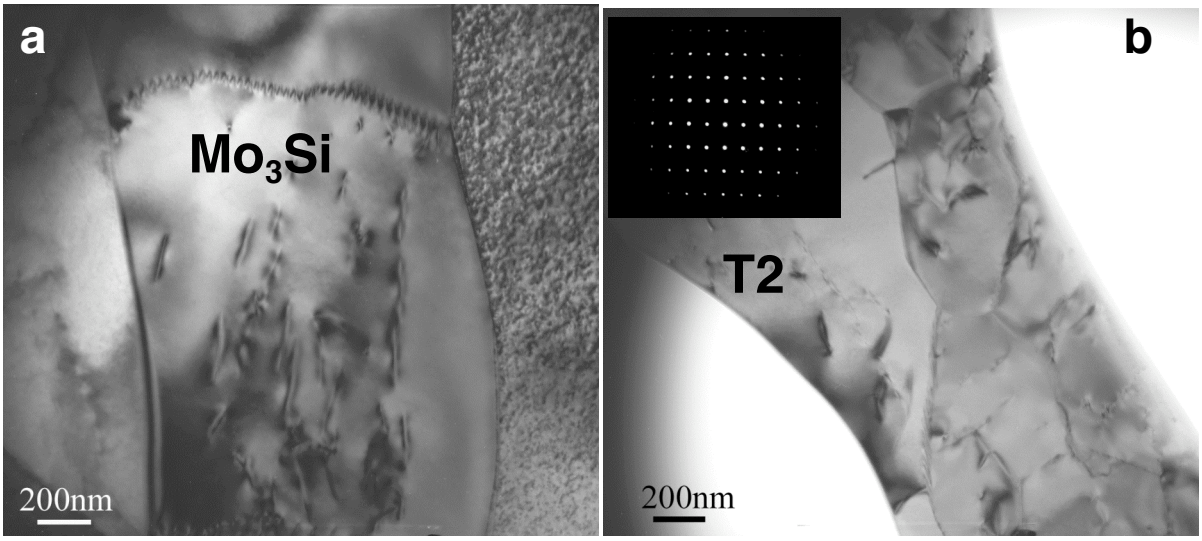

Figure 12—BF TEM micrographs showing (a) Mo_3Si grain and (b) T2-Mo_5SiB_2 grain (inset [100] T2 SAD pattern) in the Mo-3Si-1B alloy crept at 1200°C under a stress of 300 MPa.

5.2 Mo-20Si-10B (in At.%) Alloy

5.2.1 Microstructure of Undeformed Samples

The microstructures of the five processed samples (Figures 13-17) were composed of three phases appearing in bright, gray and dark contrast, which were confirmed by EDS analysis as being the α-Mo, Mo_3Si and T2-Mo_5SiB_2 phases, respectively, with the size, volume fraction and distribution of the phases varying depending on the time at 1600°C in vacuum and initial powder size prior to HIP-consolidation. Sample M1 had the lowest volume fraction of α-Mo, together with a bimodal distribution of Mo_3Si particles within a largely T2 matrix (Figure 13). The size of the intermetallic particles was largest in samples C1 and C2 and, furthermore, the α-Mo was present as a continuous network around these particles (Figures 14,15). In sample M, both the α-Mo and intermetallic phases were smaller in size, with the former again present in the form of a more or less continuous network. (Figure 16). In contrast, in sample M2 (Figure 17), the α-Mo volume fraction was smaller and far less continuous.

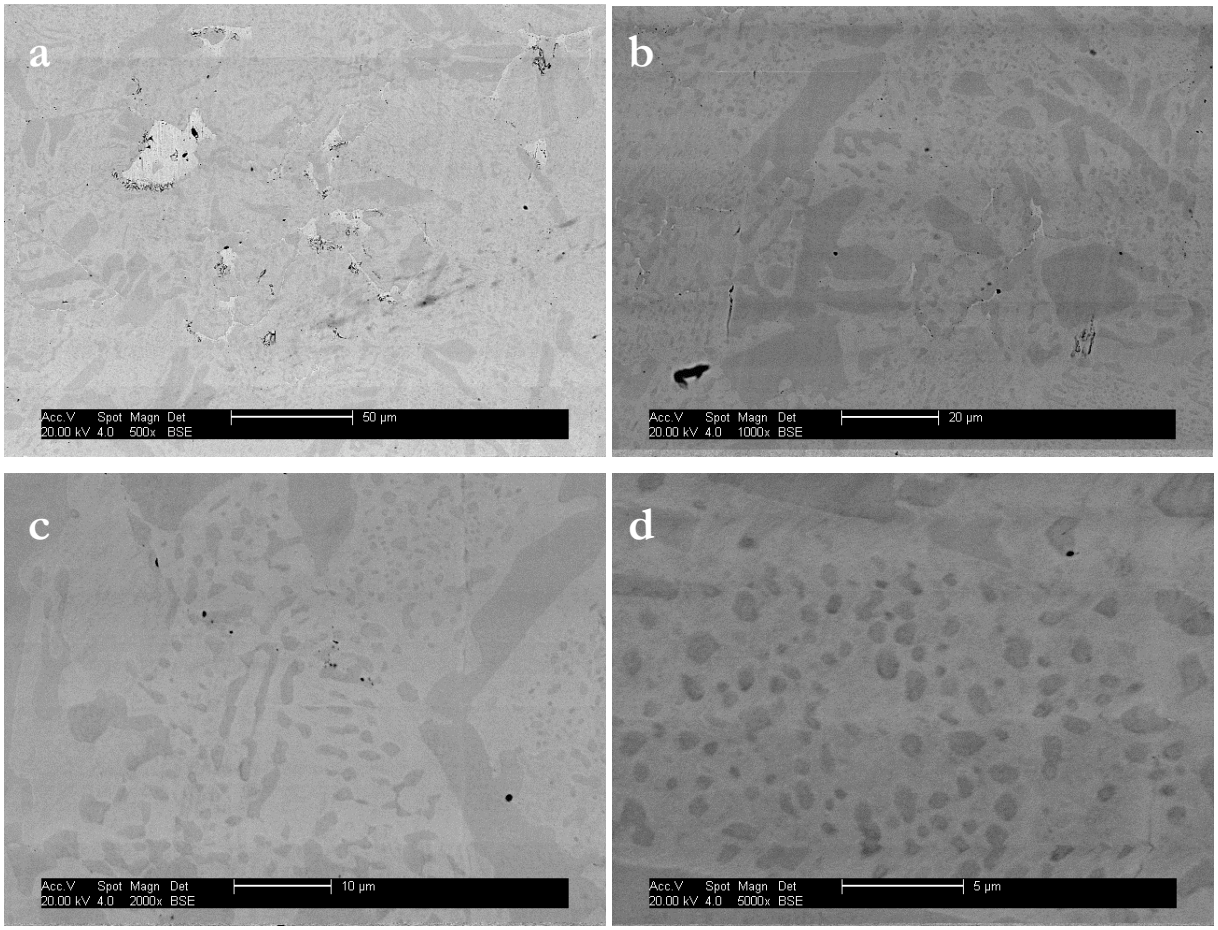

Figure 13—BSE micrographs showing microstructure of sample M1 (a) 500X, (b) 1000X, (c) 2000X and (d) 5000X.

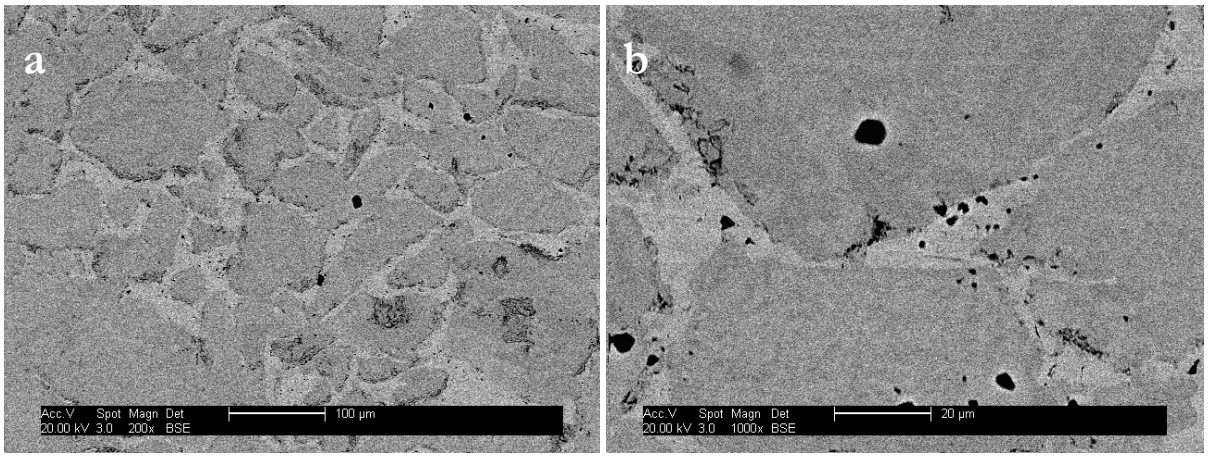

Figure 14—BSE micrographs showing microstructure of sample C1. (a) 200X and (b) 1000X.

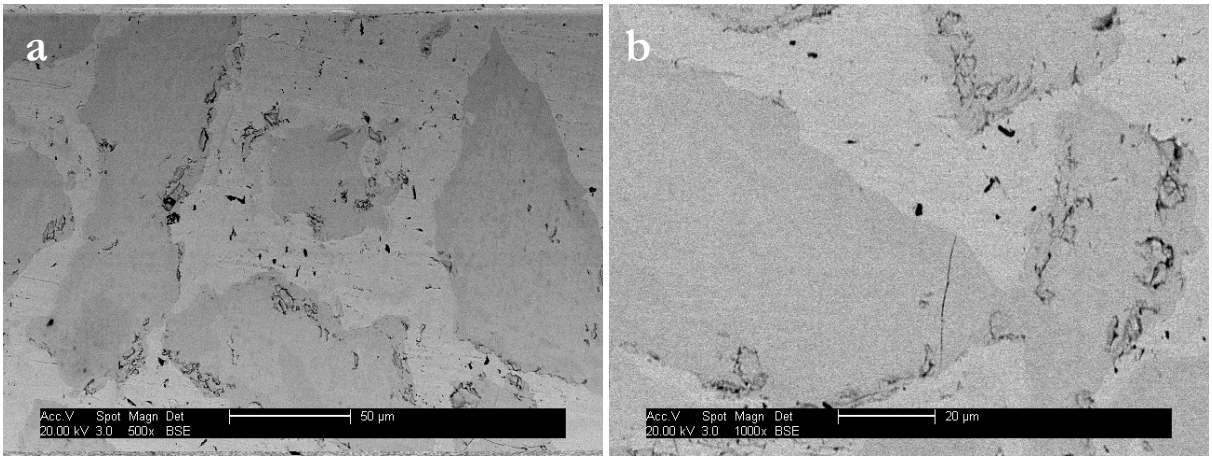

Figure 15—BSE micrographs showing microstructure of sample C2. (a) 500X and (b) 1000X.

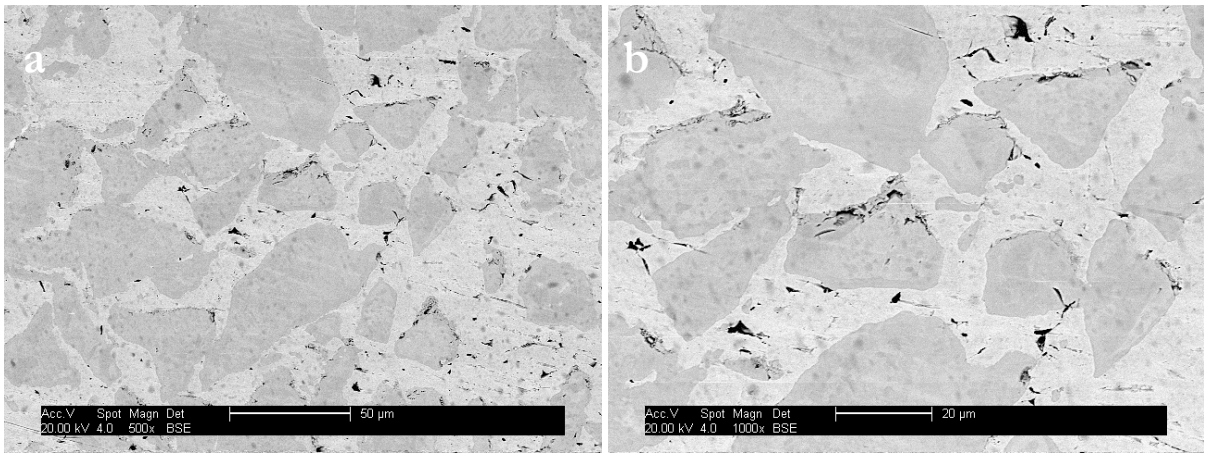

Figure 16—BSE micrographs showing microstructure of sample M (a) 500X and (b) 1000X.

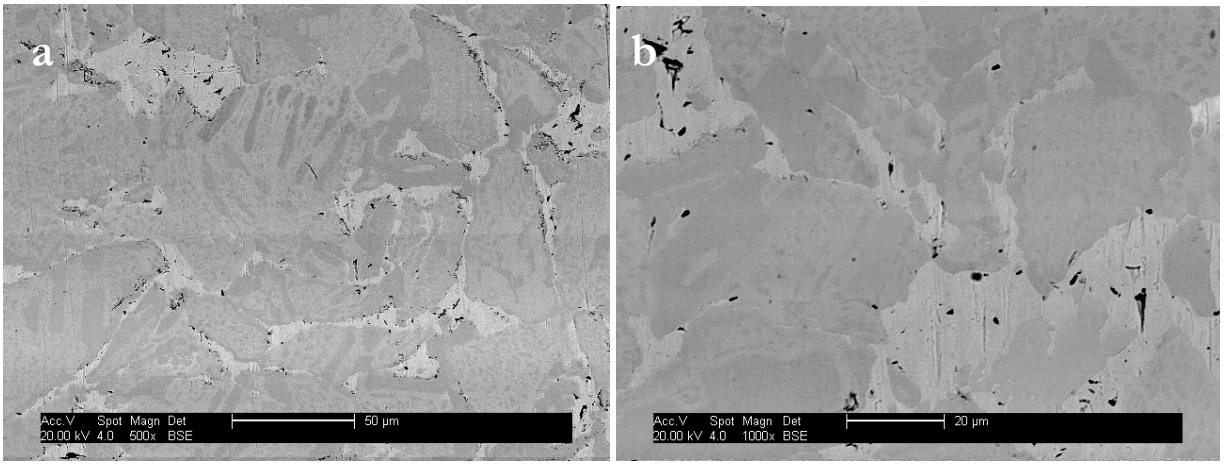

Figure 17—BSE micrographs showing microstructure of sample M2. (a) 500X and (b) 1000X.

XRD was utilized to identify the phases present in the various samples. Representation results are shown in Figure 18. In all cases, the peaks present could be associated with the α-Mo, Mo_3Si and T2 phases, with the relative intensities of the peaks from each phase varying in proportion with their amounts.

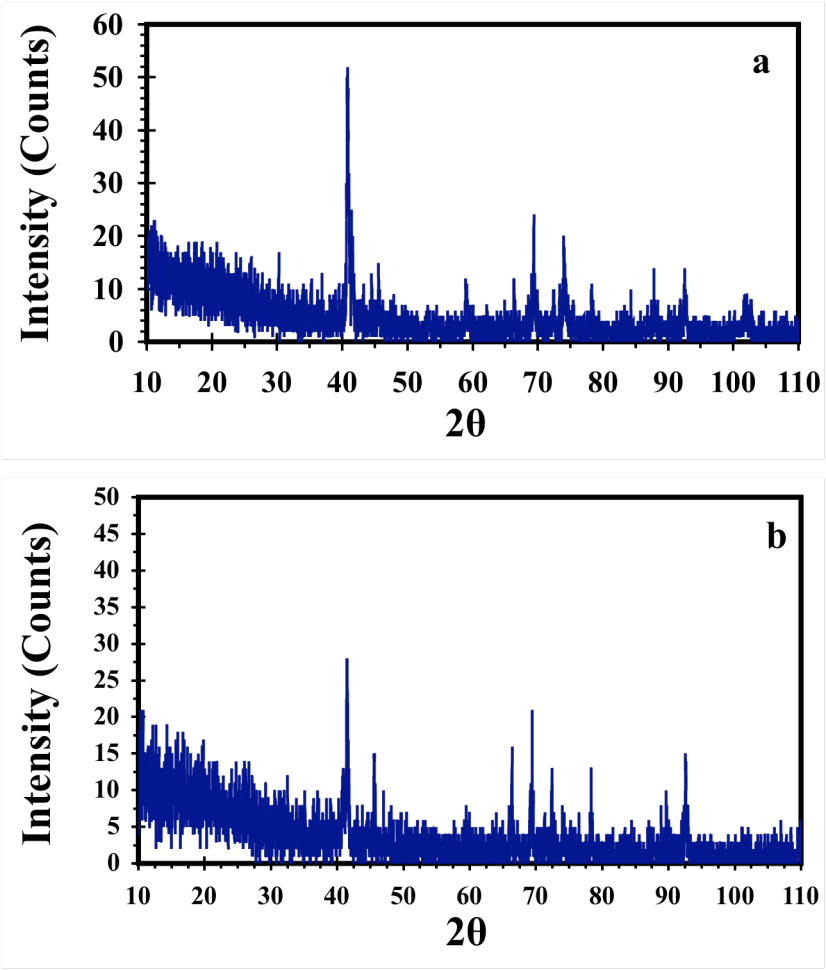

Figure 18—Plots of x-ray intensity versus 2θ recorded from various samples. (a) C1 and (b) C2.

EBSD/OIM observations in the SEM were carried out to ascertain the grain size of the α-Mo regions, Figure 19(a) shows a typical orientation map displaying the distribution of grains and Figure 19(b) displays the corresponding inverse pole figure recorded from an α-Mo region in sample C2. As can be seen, the α-Mo region (bright in Figure 15) appear to be composed of grains with sizes in the range of 1 to 4 μm (Figure 19(a)) and a majority of the grains have orientations near [101] (Figure 19(b)). The boundaries separating the grains appear to be, for the most part, low-angle.

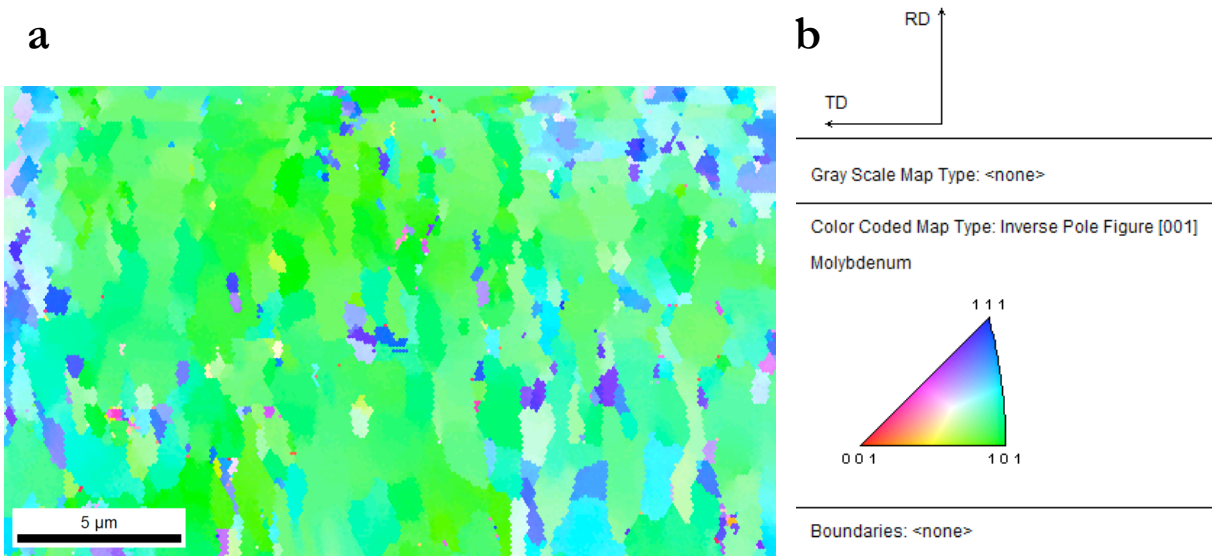

Figure 19—(a) Orientation map and (b) corresponding inverse pole figure recorded from an α-Mo region in sample C2.

5.2.2 Constant Strain Rate Compression Test Results

A typical plot of stress vs strain during a jump test is shown in Figure 20. The three segments correspond to strain rates of 10^{-6}, 10^{-5}, and 10^{-4} s^{-1}, respectively, and it can be seen that at each strain rate the initial rise in stress with strain is followed by a plateau in stress, corresponding to conditions representative of creep.

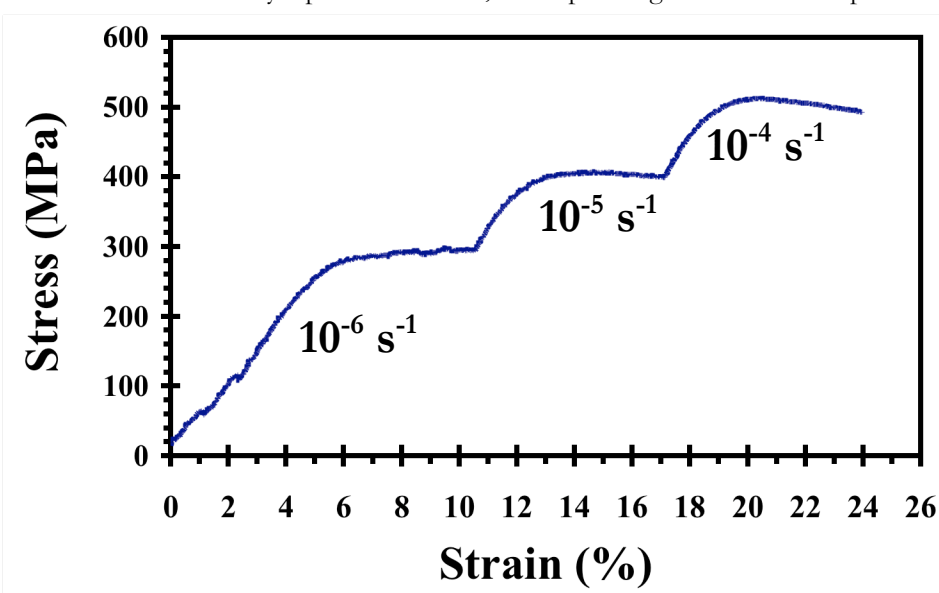

Figure 20—Plot of stress versus strain during the jump test at 1200°C for sample C1.

The data of strain rate and the corresponding plateau stress for the samples are provided in Tables 5-9 and plotted in Figure 21, together with the plateau stress corresponding to a single test at strain rate of 10^{-5} s^{-1}. As can be seen, the values of the plateau stress at the same temperature (1200, 1400°C) and strain rate (10^{-5} s^{-1}) in the jump test and single test are nearly similar to each other in almost all the samples tested, which lends confidence to the use of the jump test and the results of the plateau stress obtained therefrom. Secondly, irrespective of the α-Mo volume fraction in the sample, the plateau stress at a given strain rate generally decreases with a decrease in strain rate and with an increase in temperature. Lastly, comparing the data from the samples tested at all the three temperatures and strain rates reveals that lower the volume fraction of α-Mo, generally higher is the value of the plateau stress, especially at 1200°C. At 1400°C and the higher strain rates of $10^{-4,}$ and 10^{-5} s^{-1}, the plateau stress values do not vary much with % α-Mo (Figure 21). Log-log plots of strain rate versus stress, Figures 22 and 23, yield linear relationships, indicating that the creep behavior obeys a power law given by equation (1) at all three test temperatures in all the samples tested:

Table 5. Data of Strain Rate and Corresponding Plateau Stress at 1200, 1300 and 1400°C for Sample M1 (α-Mo – 5%).

Strain Rate (s^{-1})	**Jump Test – Plateau Stress (MPa)**		
	1200°C	1300°C	1400°C
10^{-6}	638	293	131
10^{-5}			311
10^{-4}			574

Table 6. Data of Strain Rate and Corresponding Plateau Stress at 1200, 1300 and 1400°C for Sample M2 (α-Mo – 13%).

Strain Rate (s^{-1})	**Jump Test – Plateau Stress (MPa)**			**Single Test 1200°C Plateau Stress (MPa)**	
	1200°C	1300°C	1400°C	1200°C	1400°C
10^{-6}	545	267	150		
10^{-5}	750	484	316	727	259
10^{-4}		706	507		

Table 7. Data of Strain Rate and Corresponding Plateau Stress at 1200, 1300 and 1400°C for Sample C1 (α-Mo – 17%).

Strain Rate (s^{-1})	**Jump Test – Plateau Stress (MPa)**			**Single Test 1200°C Plateau Stress (MPa)**
	1200°C	1300°C	1400°C	
10^{-6}	500	298	172	
10^{-5}	640	450	311	709
10^{-4}		578	464	

Table 8. Data of Strain Rate and Corresponding Plateau Stress at 1200, 1300 and 1400°C for Sample M (α-Mo – 34%).

Strain Rate (s^{-1})	**Jump Test – Plateau Stress (MPa)**			**Single Test 1200°C Plateau Stress (MPa)**
	1200°C	1300°C	1400°C	
10^{-6}	380	237	157	
10^{-5}	510	376	284	498
10^{-4}	619	503	450	

Table 9. Data of Strain Rate and Corresponding Plateau Stress at 1200, 1300 and 1400°C for Sample C2 (α-Mo – 46%).

Strain Rate (s^{-1})	**Jump Test – Plateau Stress (MPa)**			**Single Test 1200°C Plateau Stress (MPa)**
	1200°C	1300°C	1400°C	
10^{-6}	291	200	137	
10^{-5}	406	294	211	394
10^{-4}	512	397	301	

The values of the stress exponent, n, obtained at the three test temperatures for all samples tested as a function of the α-Mo volume fraction are listed in Table 10 and shown plotted in Figure 24. As can be seen, the n values decrease with an increase in the test temperature from 1200 to 1400°C, with the values at the latter temperature increasing from ~3 to ~6 with an increase in α-Mo volume fraction from 13 to 46%. The n values at 1200°C are much higher, in the range of ~7-9 and also do not vary much with the α-Mo volume fraction. The n values at 1300°C range from 5-7, i.e. lie in between those at 1200 and 1400°C and show a similar trend with α-Mo volume fraction as in the 1200°C data.

Table 10. Values of the Stress Exponent, n, in the Samples at Various Temperatures.

Sample ID	**α-Mo Volume Fraction, %**	**Stress Exponent, n**		
		1200°C	**1300*C**	**1400°C**
M1	5.0			3.09
M2	13.1	7.21	4.66	3.72
C1	17.0	9.33	6.82	4.58
M	34.0	9.31	6.02	4.35
C2	45.76	8.07	6.68	5.83

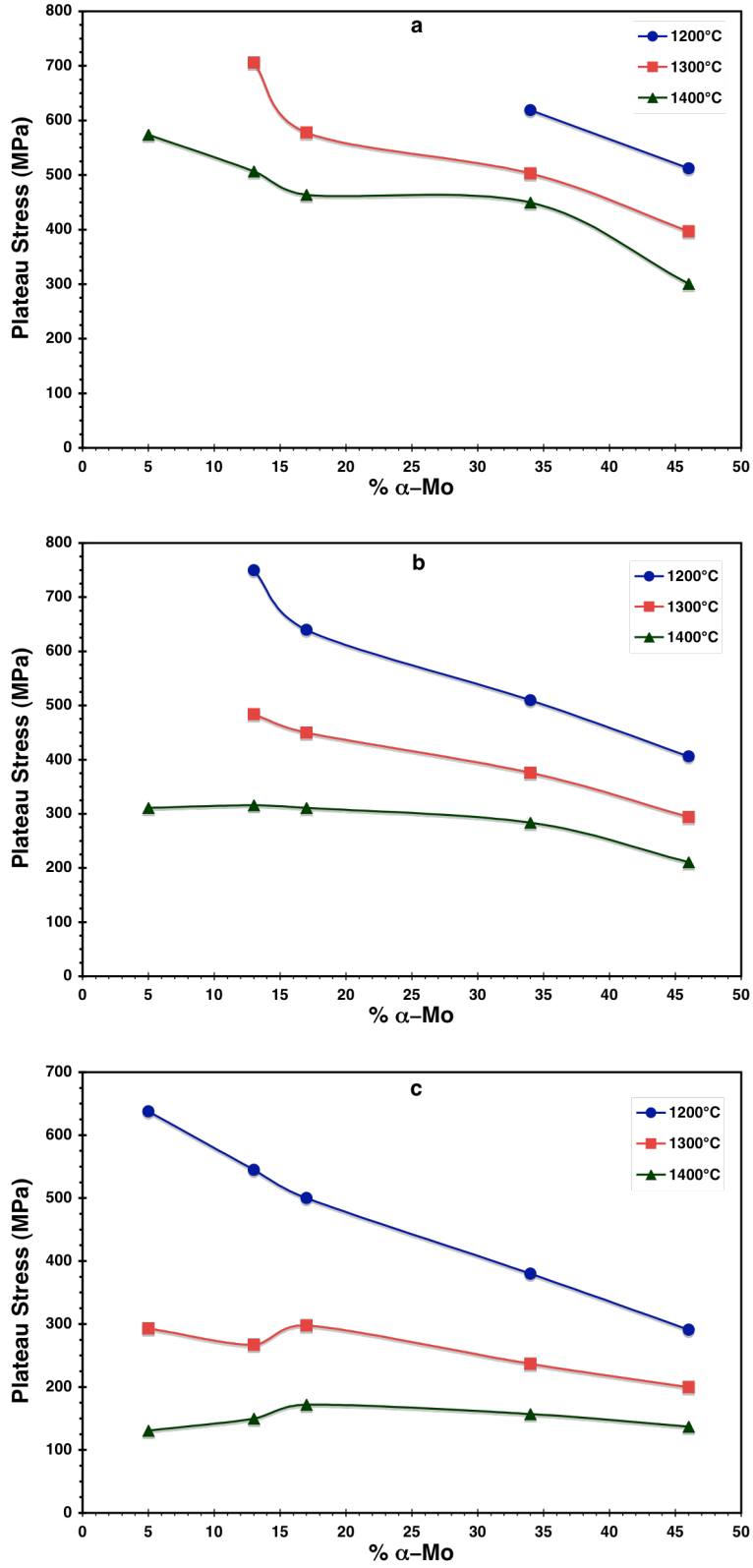

Figure 21—Plots showing the variation in the plateau stress with % α-Mo at strain rates of (a) 10^{-6} s^{-1}, (b) 10^{-5} s^{-1} and (c) 10^{-4} s^{-1}.

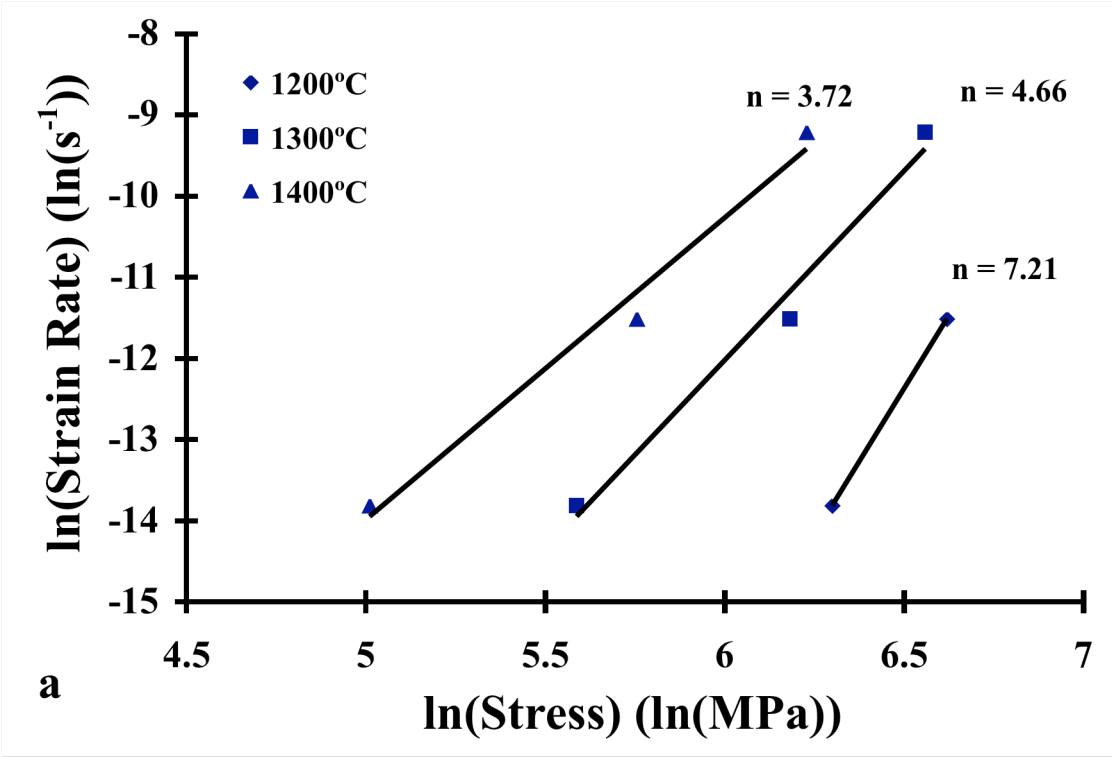

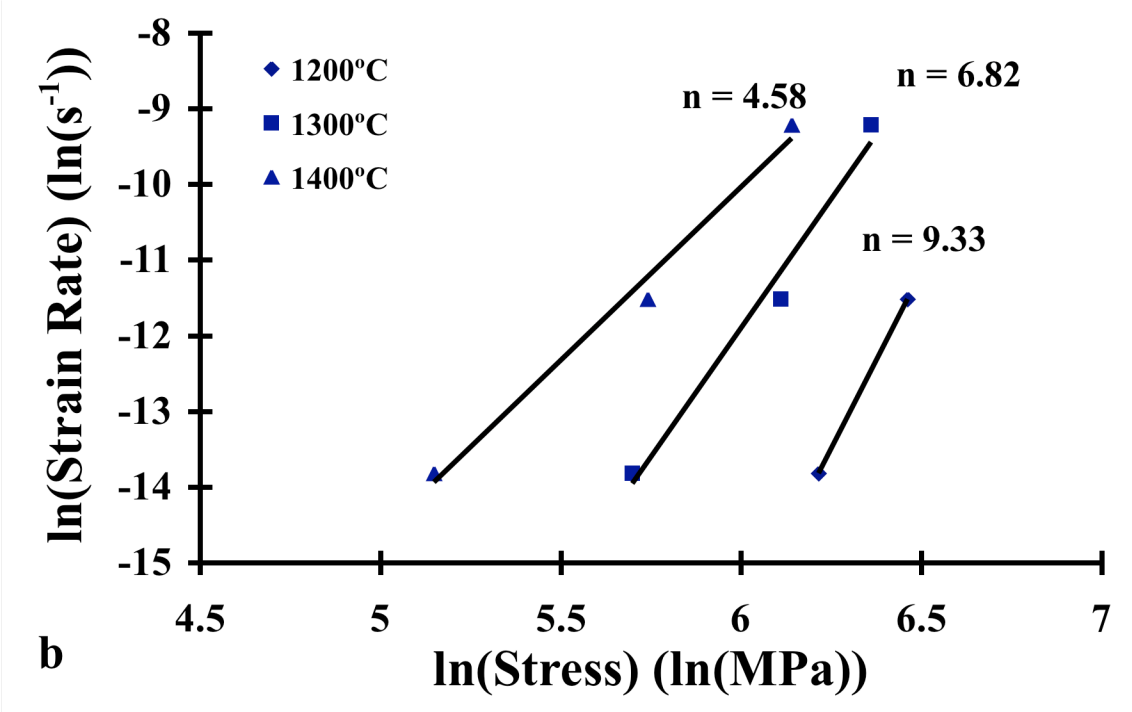

Figure 22—Plot of ln(strain rate) versus ln(stress at 1200, 1300 and 1400°C. (a) sample M2 and (b) Sample C1.

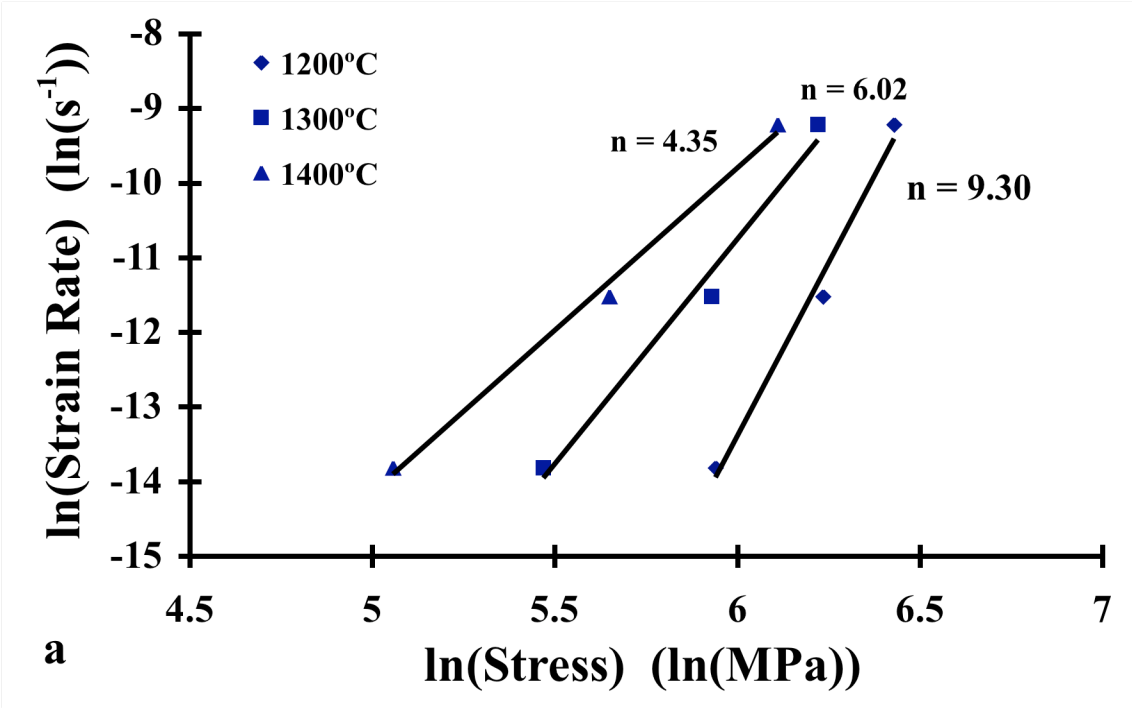

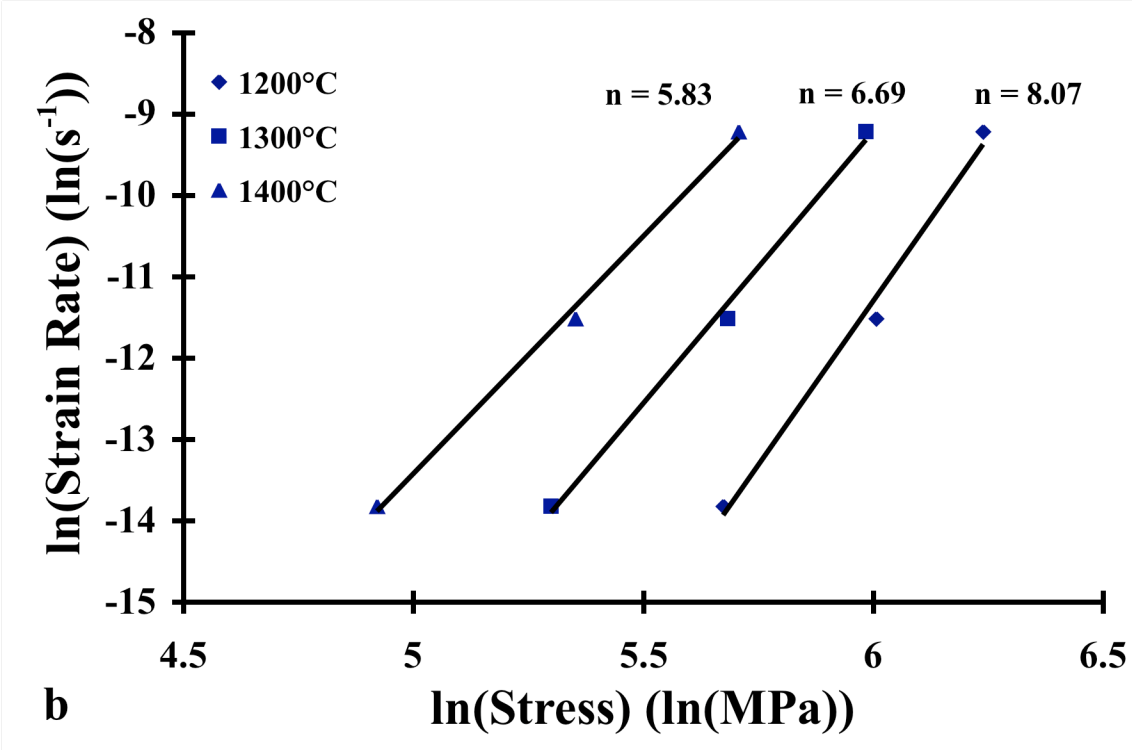

Figure 23—Plot of ln(strain rate) versus ln(stress at 1200, 1300 and 1400°C. (a) sample M and (b) Sample C2.

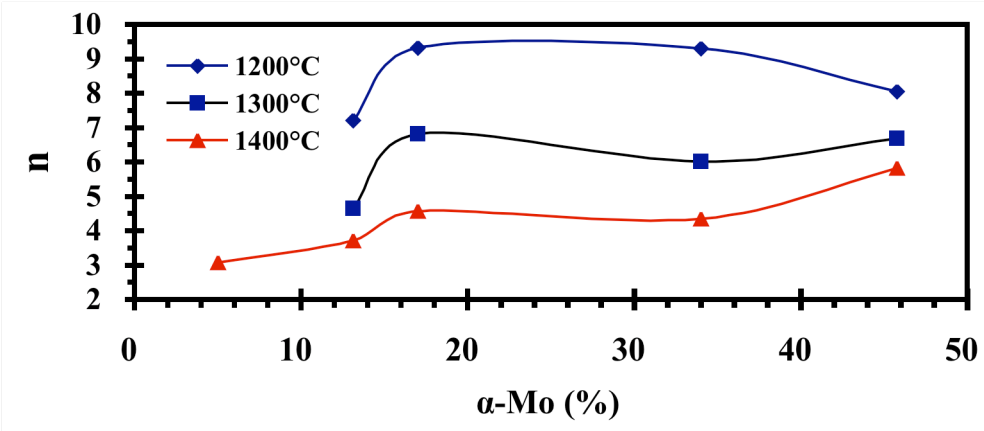

Figure 24—Plot of stress exponent values versus α-Mo volume fraction for the samples tested at 1200, 1300 and 1400°C.

Stress exponent values in the range of 3-5 expected for power law/dislocation creep, suggesting that this (i.e., dislocation climb-glide) is the dominant creep mechanism at 1400°C irrespective of the α-Mo volume fraction. This is in agreement with previous studies on compressive deformation/creep of three-phase α-Mo + Mo_3Si + T2 alloys, where stress exponents ranging from 2.1-3.9 [22] and from 2.5-7.1 [23] have been reported, though the compositions and hence volume fraction of the intermetallic phases of the alloys studied differ from that of the present work. A power law creep mechanism likely also prevails at the two lower temperatures, but the higher values of the stress exponents observed indicates that creep deformation is more difficult and that there maybe a threshold stress below which no creep occurs.

The activation energy, Q, for creep was determined from plots of ln(strain rate) versus $10^4/T$ (eqn. 1) at a given stress, a representative example of which is shown in Figure 25. In all cases, a good linear fit to the data was obtained, with the Q values calculated from the slope (=-Q/R). The Q data obtained is summarized in Table 11 and shown plotted as a function α-Mo volume fraction in Figure 26. The Q values lie in the range of ~200 to 600 kJ/mole depending on the stress level and the volume fraction of α-Mo and decrease in magnitude with an increase in both of these quantities. The values in the higher α -Mo volume fraction samples (M and C2) at 400 MPa are ~400 kJ/mole, near that for self-diffusion in α-Mo, but drop to ~200-300 kJ/mole at 600MPa. In contrast, in the lower α-Mo volume fraction samples (M1, C1), the Q values at 400 MPa are ~600kJ/mole, but drop to ~400 kJ/mole at 600 MPa. Thus, it appears that in the higher α-Mo volume fraction samples, creep is mainly controlled by deformation of the α-Mo phase and the associated diffusion-assisted climb-glide mechanisms, with the deformation process within the intermetallic particles providing a secondary contribution. In the lower α -Mo volume fraction samples, the opposite situation appears to be occurring, with the intermetallic particles controlling the deformation (and hence requiring higher stresses to produce the same strain rate) much more than the α-Mo phase, except at high stresses.

Table 11. Values of the Activation Energy as a Function of Stress in the Samples.

Sample ID	α-Mo Volume Fraction, %	Activation Energy, Q (kJ/mole)		
		400 MPa	500 MPa	600 MPa
M1	5.00	-	-	-
M2	13.10	583	503	437
C1	17.00	595	486	398
M	34.00	387	273	180
C2	45.76	395	343	302

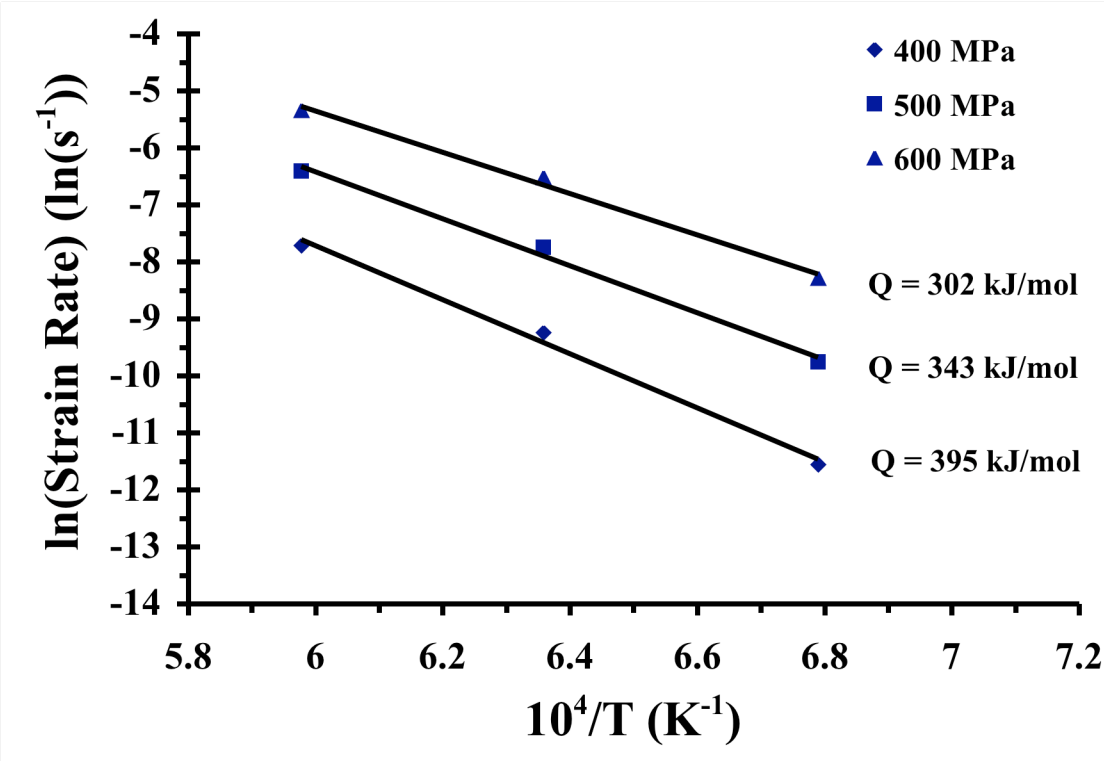

Figure 25—Plot of ln(strain rate) versus $10^4/T$ at stresses of 400, 500 and 600 MPa for sample C2, allowing determination of the activation energy, Q.

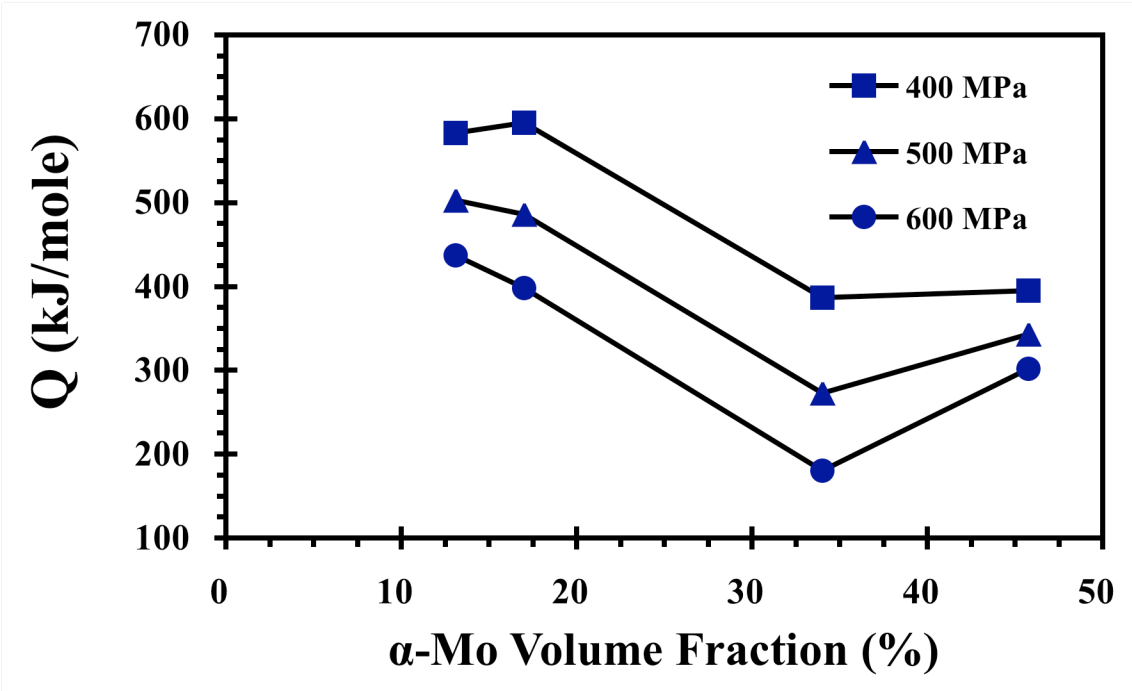

Figure 26—Plot of activation energy, Q, versus α-Mo volume fraction at different stress levels for samples tested at 1200, 1300 and 1400°C

5.2.3 Microstructure of Deformed Samples

The compression-tested samples were observed in the SEM to obtain details of the overall deformed microstructure and EBSD/OIM images of the a-Mo regions were also recorded to determine changes in grain size, if any. A typical BSE micrograph of a C2 sample tested at a single strain rate of 10^{-5} s^{-1} at 1200°C is shown in Figure 267 A change in shape of the α-Mo grains can be clearly seen, whereas the Mo_3Si and T2 particles appear relatively unchanged compared with the uncrept material (Figure15). Furthermore, many voids can be seen within the α-Mo grains, as well as cracks within the intermetallic particles and along their interfaces with the α-Mo grains. Also, subtle contrast variations can be seen with the α-Mo regions, indicative of a very fine grain size. These observations suggest that the bulk of the deformation and strain is carried by the α-Mo. Similar features were seen in the samples tested at other temperatures and strain rates, including those subjected to the jump tests. The extent of shape change of the α-Mo regions appeared a bit more pronounced in samples tested at the higher temperatures (1400°C).

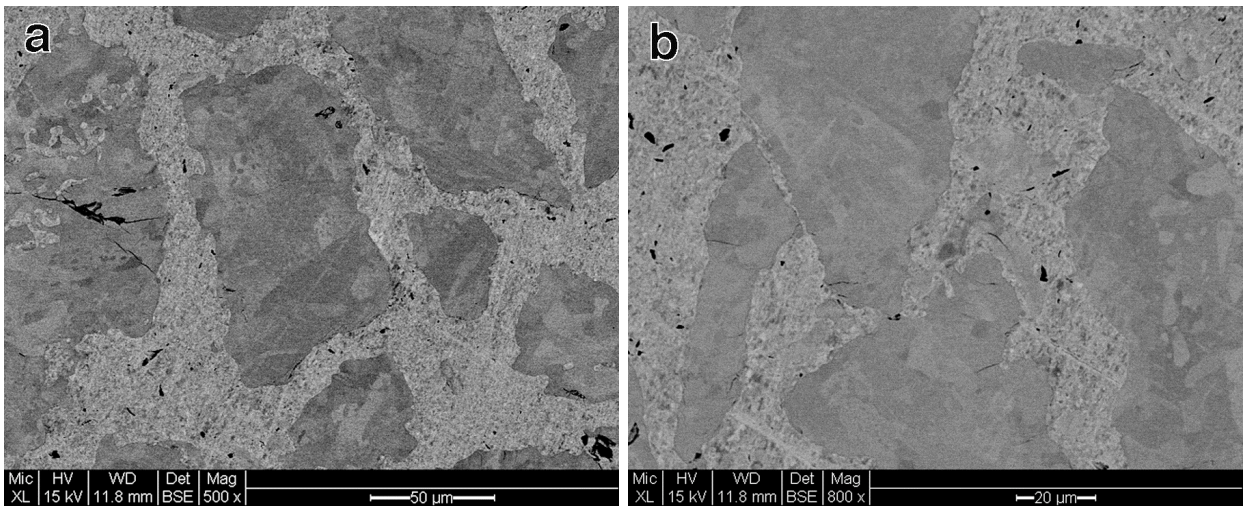

Figure 27—BSE micrographs showing overall microstructure of a C2 sample deformed at a single strain rate of 10^{-5} s^{-1} at 1200°C.

An orientation map, corresponding inverse pole figure and distribution of grain/sub-grain sizes of the α-Mo regions in the C2 sample subjected to the jump test at 1400°C are shown in Figures 28(a), 28(b), and 28(c), respectively. As can be seen, the α-Mo regions contain many fine grains/sub-grains within them and with an average size of ~0.9 μm, somewhat smaller than the average value of ~2.5 μm in the same sample in the undeformed condition (Figure 19). This reduction in the grain/sub-grain size indicates that creep processes are active during the high temperature compressive deformation.

The results of TEM observations of the same C2 sample subjected to the jump test at 1400°C are shown in Figures 29 and 30. Based on the [011] (Figure 29(a)) and [111] (Figure 29(b)) SAD patterns it was confirmed that the regions appear in bright contrast in the BSE micrographs are α-Mo. Close inspection of the α-Mo regions revealed the presence of very fine, ~1 μm size, sub-grains, confirming the OIM observations of the same in the OIM results in Figure 28, together with sub-grain boundaries composed of arrays of dislocations. Furthermore, within the sub-grains, arrays of closely-space, nearly parallel dislocations could be seen. These dislocations are visible when imaged with **g = 0-11** (Figure 30(a,b)) and **g = 101** (Figure 30(c)), but are invisible when imaged with **g = -101** (Figure 30(d)) and **g = 110** (Figure 30(e)). Based on these visibilities and invisibilities, the Burgers vector of these dislocations could be established as being **b = ½[1-11]**. Compared with the α-Mo regions, the Mo_3Si and T2 particles were found to contain very few dislocations (Figure 30(f)), indicating that the bulk of the deformation strain occurs in the α-Mo.

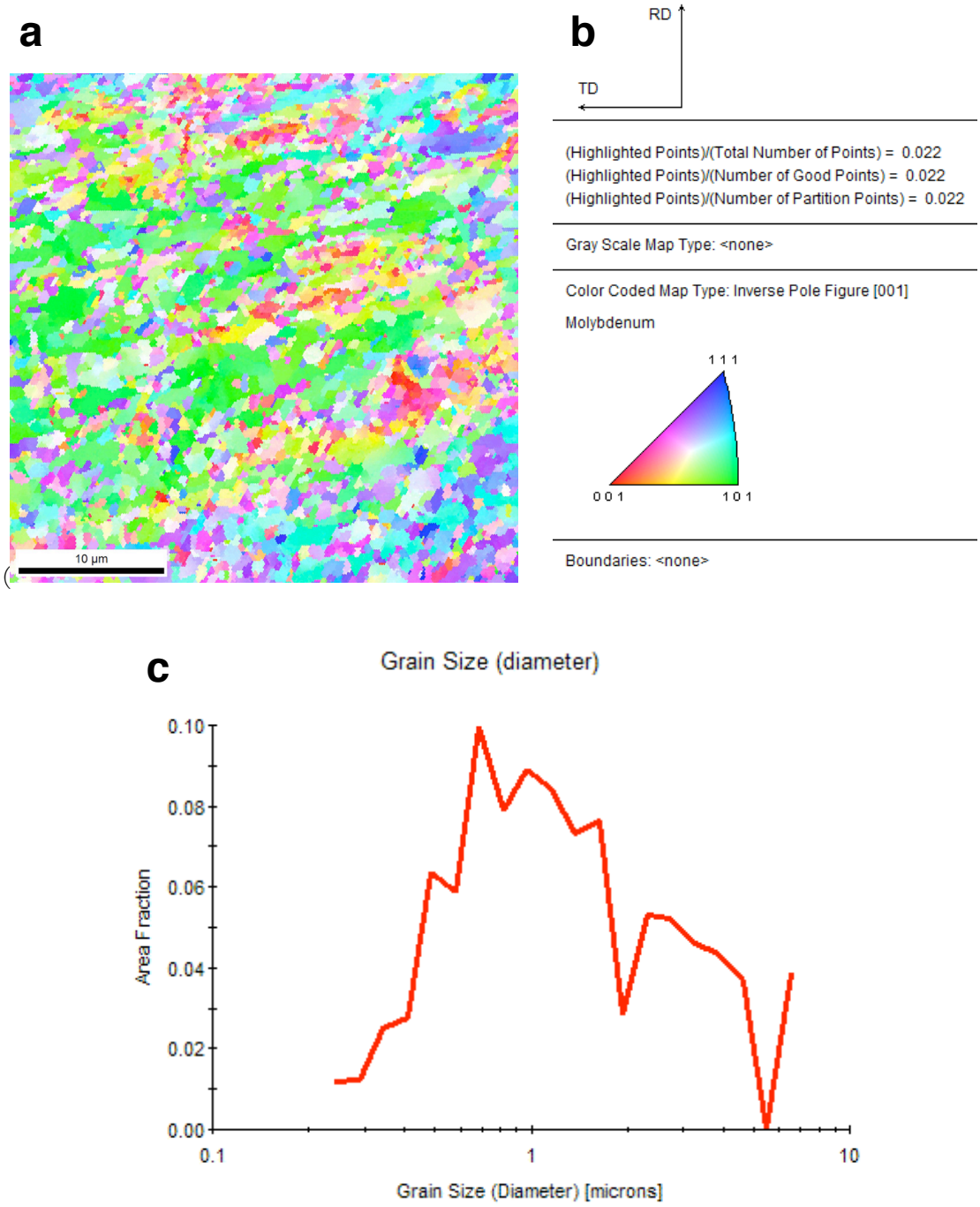

Figure 28—(a) Orientation map, (b) corresponding inverse pole figure and (c) distribution of grain/sub-grain sizes recorded from an α-Mo region in sample C2 that had been subjected to the jump test at 1400°C.

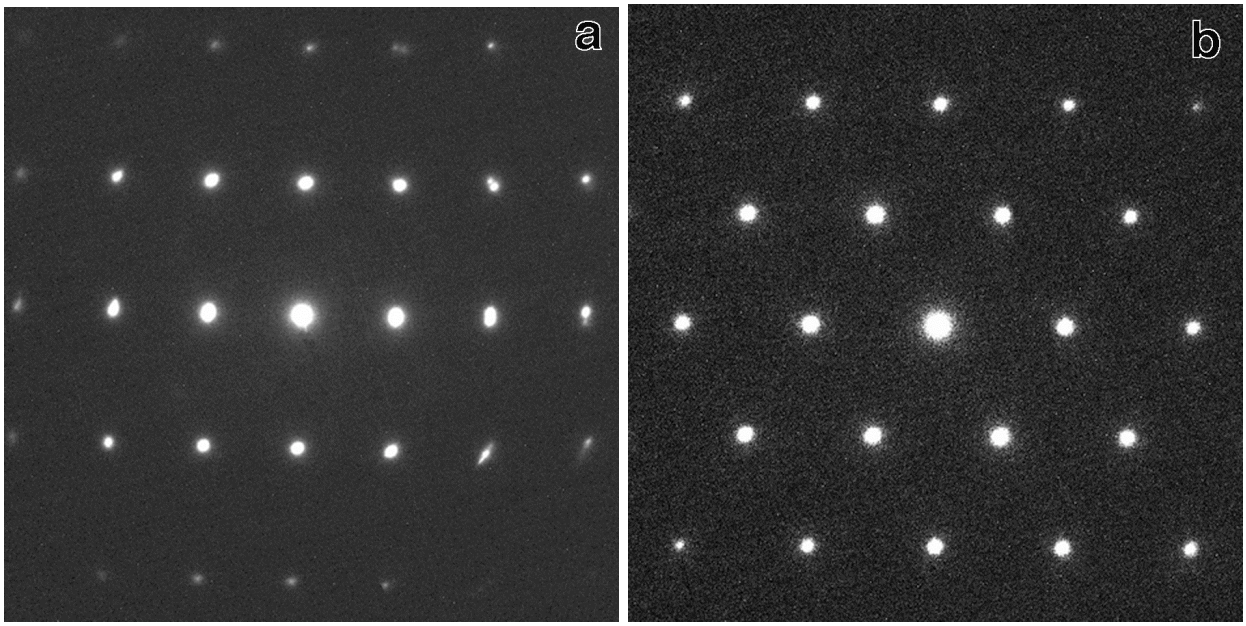

Figure 29—(a) [110] and (b) [111] SAD patterns recorded from the α-Mo region in sample C2 that had been subjected to the jump test at 1400°C.

TEM micrographs showing the α-Mo regions in the C2 sample subjected to the jump test at 1300°C are shown in Figure 31. Similar to the 1400°C tested sample, fine sub-grains (< ~1 μm wide) separated by boundaries composed of arrays of dislocations can be seen in the low magnification BF TEM micrograph in Figure 31(a). Higher magnification observations reveal many dislocations within the sub-grains. The dislocations that appear long and curved when imaged with **g = -110** (Figure 31(b) and **g = -101** (Figure 31(c)), are invisible when imaged with **g = 0-11** (Figure 31(d)) and **g = 110** (Figure 31(e)), which establishes their Burgers vector as **b = ½[1-11]**. A second set of closely-spaced dislocations having shorter segments appear in the images recorded with **g = -101** (Figure 31(b)), **g = 0-11** (Figure 31(d)) and **g = 110** (Figure 31(e), but are invisible in the image recorded with **g = -110** (Figure 31(b)), which establishes their Burgers vector to be **b = ½[-1-11]**. In contrast with the α-Mo regions, the intermetallic particles contain very few dislocations, again indicating that the bulk of the strain during high temperature compression occurs in the former.

5.3 General Discussion

The present research project has led to a number of new findings relating to the high temperature creep and compression behavior of Mo-Si-B alloys, which are discussed briefly below.

In the first part of this project, the compression creep behavior of a Mo-8.9Si-7.71Si alloy at 1100 and 1200°C and stress levels ranging from 100 to 500 MPa was studied. The results showed that at 1200°C there were two minima in the creep rate, one at small strains and the second at large strains, and the stress exponents corresponding to these minima were ~ 4 and 1, respectively. The former value compares well with the values of ~3-4 reported by others in Mo-Si-B alloys having comparable compositions [22] and indicates the dislocation climb-glide mechanisms in the α-Mo phase dominate the creep process in the early stages. Thee appears to be a transition to diffusional/recrystallization mechanisms at larger strains as suggested by the stress exponent value near 1 and TEM examination of samples crept to large strains gave evidence of the presence of recrystallized grains and many sub-grains with boundaries composed of arrays of dislocations. The creep strains were much lower at 1100°C and a stress exponent of ~2.3 was obtained, which indicates that both dislocation as well as diffusional mechanisms maybe operative. An activation energy of ~525 kJ/mole was obtained, which is somewhat higher than the value of 400 kJ/mole reported for self-diffusion in

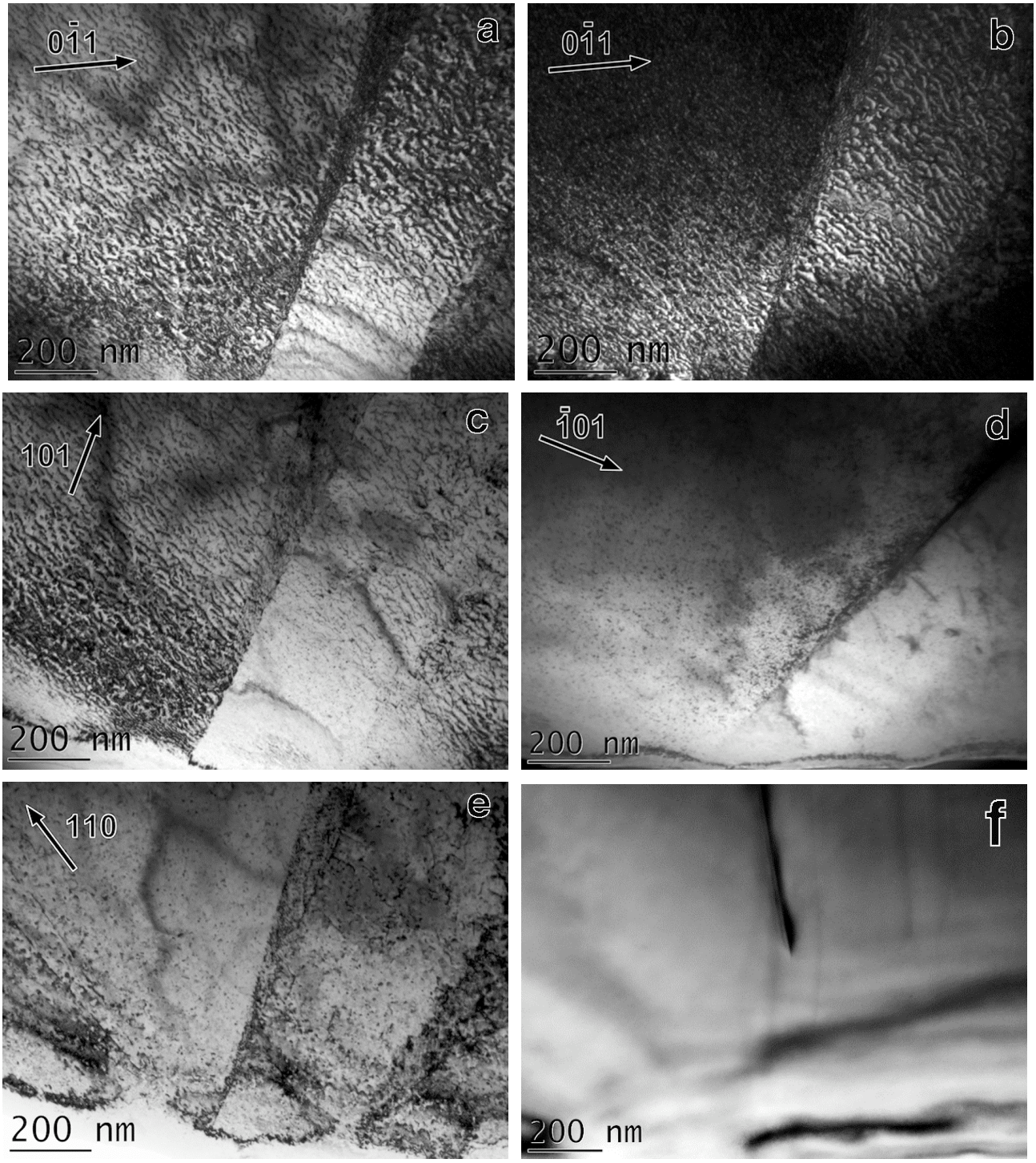

*Figure 30—TEM micrographs recorded from sample C2 that had been subjected to the jump test at 1400°C. (a) through (e) were recorded from the α–Mo region showing dislocations and sub-grain boundaries: (a) BF, **g**=0-11, (b) WBDF, **g**=0-11, (c) BF, **g**=101, (d) BF, **g**=-101and (e) BF, **g** 110; (f) BF micrograph of a Mo_3Si particle showing practically no dislocations.*

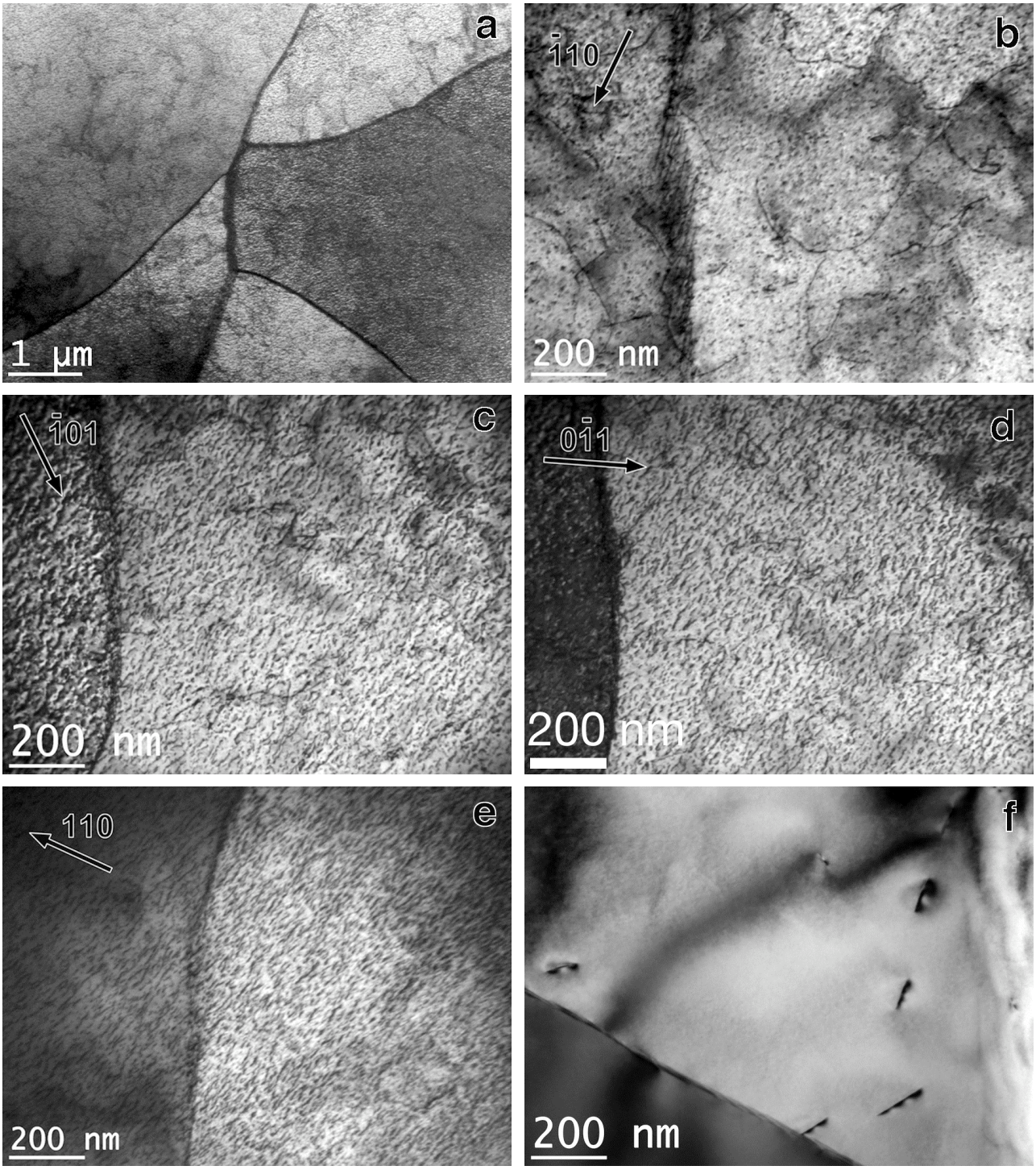

*Figure 31—BF TEM micrographs recorded from sample C2 that had been subjected to the jump test at 1300°C. (a) through (e) were recorded from the α–Mo region showing dislocations and sub-grain boundaries: (a) low magnification, (b) **g**=0-11, (c) **g**=101, (d) **g**=-101and (e) **g** 110; (f) micrograph of a Mo_3Si particle showing practical very few dislocations.*

in α-Mo. The higher activation energy maybe associated with the difficulty of plastic deformation by creep at the lower temperature of 1100°C at stresses much lower (100-300 MPa) than those of the alloy's strength (~900 MPa, Figure 4).

In the second part of the project, constant strain rate compression tests at 1200, 1300 and 1400°C of a nominally Mo-20SI-10B alloy, processed to yield five α-Mo volume fractions from 5 to 46%, were conducted. The results showed that the stresses required to maintain a given strain rate increased with a decrease in temperature and generally decreased with an increase in the α-Mo volume fraction, particularly at 1200°C. This stress did not vary much with % α-Mo at 1400°C and the two higher strain rates (10^{-5} and 10^{-4} s^{-1}). The stress exponent values were high, in the range of 7-9 at 1200°C, but lower at 1300 and 1400°C, being 5-7 and 3-6, respectively. Values of ~7 at 1200°C and ~4 at 1400°C were reported by Alur at *et al.* [23] in their study of a Mo-6.1Si-7.9B alloy utilizing the same type of constant strain rate compression tests. The activation energies were found to vary from 200-600 kJ/mole, depending on the volume fraction of α-Mo and stress level, with the higher values being obtained at the lower volume fractions and lower stress levels. These values can be compared to that of 400 kJ/mole for self-diffusion in α–Mo. The stress exponent and activation energy values do indicate that dislocation climb-glide mechanisms in the α-Mo phase dominate the high temperature deformation process. Observations of the microstructures of the deformed samples provide supporting evidence in the form of refined sub-grains and high dislocation density in the α-Mo regions, whereas the intermetallic particles show little dislocation activity and the presence of cracks.

As mentioned above, the plateau stresses are high at 1200°C and show a marked increased with an increase in the α-Mo volume fraction at the three strain rates studied. The stress exponents are also high (7-9). In comparison, the plateau stresses are much lower at 1400°C and show little or no change with an increase in the α-Mo volume fraction, i.e. micrsotructure does not exert much of an effect, and, furthermore, the stress exponents are also lower (3-6). This difference in behavior is likely to be associated with the relative plasticity of the α-Mo and intermetallic phases and the effects of temperature on the matrix/particle flow stress and plasticity. In other words, the α-Mo and intermetallic phases exhibit a temperature-dependent flow stress behavior that is sensitive to strain rate. At 1200°C, the α-Mo is likely to exhibit plasticity, whereas the intermetallic particles are elastic. Under these conditions, the intermetallic particles would constrain the deformation in the α-Mo, leading to strain accumulation/localization, work hardening and higher stresses to continue deformation, with recovery processes acting to relieve the strains and balance the stress. At 1400°C on the other hand, the flow stress and work hardening rate of the α-Mo will be lower and the intermetallic particles could also be partially plastic. The effect of this would be reduce the strain localization and stress build-up in the α-Mo and intermetallic particles and make the deformation more homogeneous and to proceed at lower stresses. Further support for these arguments can be found in the results of work by Alur *et al.* [23], who based on finite element analysis assuming an elastic-plastic α-Mo and elastic intermetallic particles, illustrated that strain localization occurs in the α-Mo to a more severe extent when the work-hardening rate decreases (i.e. increasing temperature and decreasing strain rate) while the intermetallic particles are highly stressed. On the other hand, if plastic deformation is permissible in the intermetallic particles, as would be the case at higher temperatures (1400*C) and/or lower strain rates, the strain distribution is homogenized substantially and the level of stress build-up in the particles is considerably diminished.

6. CONCLUSIONS

The main conclusions arising from the this project on the high temperature creep and compression behavior of Mo-SI-B alloys are outlined below:

Mo-8.9Si-7.71B Alloy

1. The microstructure of this alloy is three-phase, consisting of α-Mo, Mo_3Si and T2-Mo_5SiB_2 phases, with the combined volume fraction of the latter two being ~30%.

2. The elastic limit strength of the alloy remained quite high until 1200°C with a value of 800MPa, but dropped rapidly thereafter to a value of 220 MPa at 1400°C.

3. Compression creep tests showed that the creep rates at 1200°C were quite high and the creep rate versus strain data revealed two minima, the first at small strains and the second at much larger strains.

4. From the creep rate data at 1200°C, the stress exponent corresponding to the first minima was determined to be ~4.26, which is in the range of 2-7 reported for other Mo-Si-B alloys by previous investigators and indicates that dislocation climb-glide dominates the creep process in the initial stages. The stress exponent corresponding to the second minima was ascertained to be ~1.18, which is near the value of 1 and indicates that diffusional creep and/or recrystallization mechanisms dominate the creep process in the later stages.

5. From the creep data at 1100°C over the stress range of 100-300 MPa, the stress exponent was determined to be ~2.26, which suggests that both diffusional and dislocation mechanisms contribute to the creep process at this temperature and stress range.

6. The activation energy for creep was determined to ~525 kJ/mole for the Mo-3Si-1B alloy between 100 and 1200°C. This value is higher than those reported for other Mo-Si-B alloys by previous investigators and for self-diffusion (400 kJ/mole) in α-Mo.

7. Microstructural observations of post-crept samples indicated shape change and deformation of the α-Mo grains, together with the presence of many voids in these grains. A few cracks in the intermetallic particles and along their interfaces with the α-Mo matrix were also observed

8. TEM observations of the crept microstructure gave evidence for recrystallized grains of α-Mo of size 1-5 μm, as well as the presence of low-angle, sub-grain boundaries made up of dislocation arrays within these grains. The Mo_3Si and T2 grains contained a relatively low dislocation density. These various observations suggest that the bulk of the deformation and strain during creep is carried by the α -Mo and that recrystallization of this phase is responsible for the large creep strain.

Mo-20Si-10B Alloy

1. The microstructure of these samples is three-phase, consisting of α-Mo, Mo_3Si and T2-Mo_5SiB_2 phases, with the volume fraction of the α-Mo varying from 5 to ~46%.

2. The results of constant strain rate compression tests showed that the stresses required to maintain a given strain rate increased with a decrease in temperature and generally decreased with an increase in

the α-Mo volume fraction, particularly at 1200°C. This stress did not vary much with % α-Mo at 1400°C and the two higher strain rates (10^{-5} and 10^{-4} s^{-1}).

3. The values of the stress exponents determined from the data ranged from ~3-9, depending on temperature and α-Mo volume fraction, with those at 1200°C lying between 7-9 regardless of the α-Mo volume fraction, whereas those at 1400°C increased from 3 to ~6 with an increase in α-Mo volume fraction. The n values at 1300°C ranged from 5-7, i.e. were between those at 1200 and 1400°C and showed a similar trend with α-Mo volume fraction as in the 1200°C data. These stress exponent values suggest that dislocation climb-glide mechanisms dominate the creep deformation process.

4. The activation energy, Q, for creep was determined to range from ~200-600 kJ/mole, depending on the stress level and volume fraction of α-Mo.

5. OIM observations of the post-test specimens revealed very fine sub-grains (size ~1 μm) in the α-Mo, which was confirmed by TEM. In addition a high density of 1/2<111> dislocations and sub-grain boundaries composed of dislocations were observed in the α-Mo, which all provide supporting evidence for the operation of dislocation climb-glide mechanisms, consistent with the measured stress exponents and activation energies.

6. The above results suggest that the bulk of the deformation and strain during high temperature compression is carried by the α-Mo, with dislocation creep/climb-glide mechanisms being operative, with the intermetallic particles providing a varying level of constraint to the deformation and strain localization depending on temperature and strain rate, which is reflected in the flow/plateau stresses and stress exponents.

7. REFERENCES CITED

1. D. M. Dimiduk, M. G. Mendiratta and P. R. Subramanian, *In: Structural Intermetallics*, R. Darolia *et al.* (eds.), TMS-AIME, Warrendale, PA, pp. 619-630 (1993).
2. D. M. Berczik, "Method for Enhancing the Oxidation Resistance of a Molybdenum Alloy, and a Method of Making a Molybdenum Alloy," *US Patent # 5,595, 616*, January 21 (1997).
3. D. M. Berczik, "Oxidation Resistant Molybdenum Alloy," *US Patent 5,693,156* (1997).
4. M. K. Meyer and M. Akinc, *J. Amer. Cer. Soc.*, **79**, pp. 938-944 (1996); ibid pp. 2763-2766; M. K. Meyer, M. J. Kramer and M. Akinc, *Adv. Mater.*, **8**, 85-88 (1997); A. J. Thom, M. K. Meyer, M. Akinc and Y. Kim, *in: Processing and Fabrication of Advanced Materials for High Temperature Applications – III*, T. S. Srivatsan and V. A. Ravi (eds.), TMS, Warrendale, PA, pp. 413-420 (1993).
5. M. K. Meyer, M. J. Kramer and M. Akinc, *Intermetallics*, **4**, pp. 273-281 (1996).
6. C. A. Nunes, R. Sakidja and J. H. Perepezko, *In: Structural Intermetallics*, M. V. Nathal *et al.* (eds.), TMS, Warrendale, PA, pp. 831-839 (1997).
7. C. A. Nunes, R. Sakidja, Z. Dong and J. H. Perepezko, *Intermetallics*, **8**, pp. 327-337 (2000).
8. R. Sakidja, J. Meyers, S. Kim and J. H. Perepezko, *Int. J. Refract. Met. & Hard Compounds*, **18**, pp. 193-204 (2000).
9. M. G. Mendiratta, P. R. Subramanian and D. M. Dimuduk, *Intermetallics*, **10**, pp. 225-232 (2002).
10. T. A. Parthasarathy, M. G. Mendiratta and D. M. Dimuduk, *Acta Mater*, **50**, pp. 1857-1868 (2002).
11. J. H. Schneibel, C. T. Liu, D. S. Easton and C. A. Carmichael, *Mater. Sci. Eng*, **A261,** pp. 78-83 (1999).

12. C. T. Liu, J. H. Schneibel and L. Heatherly, *Mat. Res. Soc. Symp. Proc.*, **552**, pp. 246-251 (1999).

13. I. Rosales, J. H. Schneibel, *Intermetallics*, **8**, p. 885 (2000).

14. R. D. Field, D. J. Thoma, J. C. Cooley, F. Chu, C. L. Fu, M. H. Yoo, W. L. Hults, C. M. Cady, *Intermetallics*, **9**, p. 863 (2001).

15. K. Ito, K. Ihara, K. Tanaka, M. Fujikara and M. Yamaguchi, *Intermetallics*, **9**, p. 591 (2001).

16. K. Yoshima, M. H. Yoo, A. A. Wereszczak, S. M. Borowicz, E. P. George, R. H. Zee, *Scripta Mater.*, **45**, p. 1321 (2001).

17. T. G. Nieh, J. G. Wang and C. T. Liu, *Intermetallics*, **9**, pp. 73-79 (2001).

18. J. H. Schneibel, M. J. Kramer, O. Unal and R. N. Wright, *Intermetallics*, **9**, pp. 25-31 (2001).

19. H. Choe, D. Chen, J. H. Schneibel and R. O. Ritchie, *Intermetallics*, **9**, pp. 319-329 (2001).

20. J. H. Schneibel and H. T. Lin, *Materials at High Temperature*, **19**, pp. 25-28 (2002).

21. J. H. Schneibel, M. J. Kramer and D. S. Easton, *Scripta Mater.*, **46**, pp. 217-221 (2002).

22. J. H. Schneibel, *Intermetallics*, **11**, 625-632 (2003).

23. A. P. Alur, N. Chollacoop and K. S. Kumar, *Acta Mater.*, **52**, 5571-5587 (2004).

8. List of Publications, Presentations and Students Supported From the Grant

8.1 Publications and Presentations

Four papers based on the results obtained were presented at the 2005 and 2006 TMS/ASM Fall Meetings held in Pittsburgh, PA and San Diego, CA, respectively, the 2007 Annual Meeting held in Orlando, FL and the MS&T 2008 Fall Conference held in Pittsburgh, PA. Two articles based on the results are being prepared for submission to the journals *Intermetallics* and *Acta Materialia*.

8.2 Students Supported Under this Grant

Brian Riestenberg and Xingshuo Wen, M S. students in the Department of Chemical and Materials Engineering, University of Cincinnati.

9. Acknowledgements

The authors thank DoE-NETL for financial support of this research under grant # DE-FG-03NT41793, with Dr. Richard B. Read as Project Officer. Appreciation is also extended to Dr. Joaquim Schneibel from ORNL for providing samples of the Mo-20Si-10B alloy for the project and to Dr. K. Sharvan Kumar and Mr. Padam Jain from Brown University for use of the creep equipment there and help in the creep testing of these samples. The authors also wish to thank Dr. Madan Mendiratta for supplying the materials in the earlier parts of this study and for helpful discussions in guiding the work, In addition, the authors thank the AFRL for use of the sample, preparation, creep testing and characterization facilities, as well as Mr. Mike Scott from UES/AFRL for his help with the creep testing..